Analysis of Natural Convective Flow of Casson Fluid around an Inclined Rectangular Cylinder

Olalekan Adebayo Olayemi[1,2]*, Tomisin Favour Ajide[1], Adebowale Martins Obalalu[3], and Muneer A. Ismael[4,5]

[1]Department of Aeronautics and Astronautics, Kwara State University, P.M.B. 1530, Malete, Kwara State, Nigeria.

[2]School of Engineering, Cranfield University, Cranfield, MK43 0AL, United Kingdom.

[3]Department of Physics, Augustine University, Ilara-Epe, Lagos State, Nigeria.

[4]Mechanical Engineering Department, Engineering College, University of Basrah, Basrah, Iraq.

[5]College of Engineering, University of Warith Al-Anbiyaa, Karbala, Iraq

*Corresponding author. Tel.: +447424001433.

Email address: olalekan.a.olayemi@cranfield.ac.uk, olalekan.olayemi@kwasu.edu.ng

Abstract

The current investigation uses the finite element method to analyze the natural convective flow of Casson fluid around a tilted hot rectangular cylinder placed in a square container. The influence of Casson fluid parameter (η), aspect ratio, (AR), angle of tilt (γ), and Rayleigh number (Ra) on isotherms and fluid flow pattern is enunciated. The walls of the enclosure and that of the cylinder are respectively fixed as T_c and T_h. Results from the findings reveal that for the range of Casson fluid parameter $(0.1 \le \eta \le 1.0)$, aspect ratio $(0.1 \le AR \le 0.7)$, and Rayleigh number $(10^3 \le Ra \le 10^6)$, investigated, the rate of heat transfer of the enclosure wall increases with increasing η, AR and Ra, while for the heated rectangular obstacle, the rate of heat transfer decreases with AR growth but improves with the growth of η and Ra. At $Ra = 10^6$, improvement in γ results in heat transfer enhancement for both the enclosure and cylinder walls. However, for Ra in the interval of $10^3 \le Ra \le 10^5$, the response of the thermal profiles of both the rectangular cylinder and enclosure walls to cylinder orientation depends on the values of Ra and γ considered.

Keywords: Casson fluid; Natural convection; rectangular cylinder; Aspect ratio; square enclosure.

Nomenclature

AR	aspect ratio, W / L	W	dimensionless width of the cylinder
$e_{i,j}$	(i, j) components of deformation rate	X, Y	dimensionless Cartesian coordinates
H	dimensionless height of the rectangular cylinder	α	thermal diffusivity, m^2 / s
L	dimensionless height of the square cavity	γ	inclination angle
$\overline{Nu}$	average Nusselt number	$\dot{\gamma}$	shear rate, s^{-1}
Nu_L	local Nusselt number	η	Casson fluid parameter
P_y	fluid yield stress, N / m^2	μ_B	plastic dynamic viscosity, Ns / m^2
P	dimensionless pressure	π	deformation rate, s^{-1}
Pr	Prandtl number	π_c	the critical value of deformation rate
q	heat flux, W / m^2	ρ	fluid density, k / gm^3
Ra	Rayleigh number	τ	shear stress, N / m^2
T	temperature, K	φ	dimensionless temperature
U, V	dimensionless velocity components	ψ	stream function, kg / ms

1. Introduction

Natural convection is a kind of heat transport mode whereby fluid motion is not aided by any external force but results solely due to density difference which arises from a gradient in temperature [1]. Natural convection can be grouped into two categories based on the pattern of fluid flow and geometry namely internal and external convection [2]. In internal flows, fluid motion is bounded by solid boundaries while in external flows, fluid motion is around a solid boundary [3]. Natural convection in external flows is easier to analyze than those occurring in internal flows; and also, problems in internal natural convection can be divided into two classes based on the thermal boundary conditions imposed; these are cavities whose side walls are cooled or heated, and those with heated lower walls [4–6]. In many industrial applications, natural convection is crucially important, for example, in electronic equipment cooling, solar collectors, heat exchangers, lubrication systems, solar water desalination , electric furnaces, melting and freezing processes in the engineering field and ,in nuclear reactors [7–12]·

In heat transfer, the fluid used as the working fluid is very important as it can contribute to heat transfer enhancement [13–16]· Generally, working fluids are categorized into Newtonian and non-Newtonian fluids. Research has shown that non-Newtonian fluids possess much more rheological properties than Newtonian ones and are therefore more beneficial in biomedical engineering, chemical engineering, colloidal liquids, and several other fields [17–19]. The Casson fluid model, which was introduced by Casson in 1959 to analyze pigment and oil mixture, is among the most widely used viscoplastic non-Newtonian fluid models [20–22]. Essentially, there are three basic viscoplastic models namely, the Casson, Herschel-Bulkley and Bingham models [23]. Furthermore, using the Casson model, the flow dynamics of some particulate suspensions can be accurately described [24]. Also, the production of petroleum, paints, sewage, soup, and lubricants can also be described by the Casson Model [18, 25]. Based on the rheological significance of the Casson fluid model, a lot of researchers have investigated Casson fluid flow over plates or points of stagnation [26]. However, there is a paucity of work on natural convective flow of Casson fluid in enclosures [27]. Some of the recent investigations on the Casson fluid model include [28–33]. It is imperative to submit that in most of these investigations, the partial differential equations governing Casson fluid flow have been reduced with the aid of similarity transformation parameters into ordinary differential equations and Casson fluid properties rendered as fixed coefficients while the Newtonian fluid relations were used to approximate the stress-deformation behaviour [9, 34].

Efforts made by some researchers in natural convection includes [8] who used both the Bingham and Casson models to investigate the thermal and velocity profiles of a heated square enclosure which contained a yield stress fluid. The results showed that the level of shear-thinning in the Bingham fluid scenario is higher than that of the Casson model and featured supercritical bifurcation at the point of transition between convection and conduction regions. The implications of thermal radiation and viscosity in the natural convection of Casson fluid in a heated square cavity was considered by [9]. It was revealed that increasing the Casson parameter resulted in heat transfer augmentation and strengthening of the velocity profile. Casson fluid flow under mixed convective condition in a wavy bottom wall trapezoidal enclosure whose top and lower boundaries were sustained at high temperature was analyzed by [10]. It was reported that Richardson number improvement augmented heat transfer for the various Casson fluid parameter considered. [12] explored the influence of *AR*, entropy generation, and thermal radiation on natural convection in a rectangular box containing Casson fluid. It was discovered that improvement in radiation parameter reduced thermal energy transport but was enhanced with rising Casson parameter. The Marker and Cell approach was used by [35] to simulate Casson fluid in a square enclosure under the influence of buoyancy force. The outcome shows that increasing *Ra* resulted in convection strengthening for all the values of the Casson fluid parameter considered.

Similarly, the Adomian decomposition and the variation iteration methods were used to study the impacts of Reynolds number, Peclet number, and angular velocity on the thermal and micropolar fluid flow profiles between two parallel plates. The investigation submitted that heat transfer was augmented by increasing the Peclet number and the fluid concentration while the Reynolds number increment favoured the thickening of the velocity boundary layer [36]. In addition, an investigation of conduction heat transfer via a vertical channel was done by [37] using the Finite Element, and the Akbari Ganji's Methods; it was reported that increasing the thermal conductivity of fluid enhanced the fluid flow, and the thermal profile of the channel. The flow of Maxwell-TiO_2 nanofluid over a stretching surface having rectangular, triangular, and chamfer blades incorporated into it was considered and one of the major conclusions was that the TiO_2 velocity at the entrance of the stretching surface was highest with the rectangular bladder configuration [38]. The velocity and temperature variations along the axial direction in various baffle configurations under the influence of a magnetic field were analysed and the analysis revealed that the rectangular baffle augmented heat transfer the most [39]. The impact of Maxwell nanofluid flow with MWCNT nanotubes over a stretching sheet with two circular wires carrying opposite currents was studied by [40].The report provided information on the velocity distribution along different sections of the sheet

The convective flow of Casson fluid with carbon nanoparticle inside a partially heated wavy enclosure containing a circular obstruction situated inside it under the influence of thermal radiation was reported by [41]. It was submitted that the mean Nusselt number was higher when the obstacle was cold, also the rate of heat transfer of the wavy wall was enhanced as the Casson-Fluid parameter improved. Numerical investigation into the thermal management of conjugate heat transfer of a curved solid conductive panel having various cooling systems was conducted by [42]; several conclusions were drawn and one of it upheld that thermal performance of the system declined with the increase in the diameter of the nanoparticles. The Finite Element Method was used to investigate the thermal and flow behaviours of Ag/ H_2O nanofluid which is contained in a porous square enclosure under the influence of a magnetic force, and some of the key conclusions were that the mean Nusselt number along the heated wall improved as the nanoparticle volume fraction increased, and that total entropy generation was enhanced by increasing the Darcy number [43].

The influence of ternary nanoparticles on hyperbolic tangent material to unravel its thermal performance was looked into by [44]. The Galerkin Finite Element Method was used to implement the governing equations of flow and heat transfer. Two of the key conclusions were that tri-hybrid nanoparticles transferred more heat compared to hybrid nanostructures and nanoparticles; and that high Weissenberg number value and magnetic number were used to inhibit fluid motion. A novel method (viscoplastic and micropolar models) was used by [45] to investigate the influence of particle rotation in the Cosserat-Maxwell boundary layer flow. Some of the pertinent conclusions made from the study were that the Newtonian and Cosserat-Maxwell fluids yielded higher heat transfer rates compared to that yielded in classical-Newtonian and classical-Maxwell fluids. Also, it was opined that thermal and momentum relaxation characteristics have some significance in the restoration of thermal and fluid equilibria.

Though concerted efforts have been made to investigate the flow of Casson fluid particularly around solid boundaries and very few works on convection in internal enclosures [46]. Based on the literature search conducted by the authors, no work had been reported on the thermal and fluid flow profiles of Casson fluid around a rectangular cylinder located concentrically inside a cold square enclosure. Thus, it is sought that this paper participates in discovering the implications of using Casson fluid in conveying energy from a hot cylinder to a cold wall. This investigation finds application in petroleum engineering such as in crude oil extraction from the product of petroleum, biomedical medical engineering such as in blood flow, in the paper and drug industry, etc. The geometry used for the present study was chosen because no previous study had considered such a geometry; Furthermore, the thermal and fluid flow information provided by this analysis will be useful for both research and industrial purposes.

2. Methodology

2.1 Description of the physical Model

In the current work, the geometry and the coordinate system employed are as presented in Figure 1 while Figure 2 shows the mesh distribution of the model. The physical model is made up of an inclined rectangular cylinder placed concentrically inside a square domain. H, is the height of the rectangular cylinder with aspect ratio, $AR = \frac{W}{L}$, while each of the enclosure wall length is L. The annulus in the model is filled with Casson fluid with Prandtl number, $\mathrm{Pr} = 6.8$. The height of the rectangular cylinder is taken to be fixed $\left(H = 0.1L\right)$; the fluid flow and heat transfer profiles are presumed to be $2-D$. The flow in the annuli is non-Newtonian, laminar and equipped with natural convection flow mechanism. The solid boundaries of the enclosure are held at a fixed cold temperature (T_c) while the obstruction is maintained at a hot constant temperature, (T_h). The properties of fluid are taken to be fixed except density, which follows the Boussinesq approximation. All the solid boundaries in the adopted model are maintained at a fixed zero velocity.

The rheological equation of state for an isotropic and incompressible flow of Casson fluid is expressed by following [35, 47]

$$\tau^{\frac{1}{2}} = \tau_o^{\frac{1}{2}} + \mu \dot{\gamma}^{\frac{1}{2}} \tag{1}$$

$$\tau_{ij} = \begin{cases} 2(\mu_\beta + \frac{p_y}{\sqrt{2\pi}})e_{ij}, \pi > \pi_c \\ 2(\mu_\beta + \frac{p_y}{\sqrt{2\pi}})e_{ij}, \pi > \pi_c \end{cases} \tag{2}$$

The relevant non-dimensional governing equations are as follows.

Continuity:

$$\frac{\partial U}{\partial X}+\frac{\partial V}{\partial Y}=0 \qquad (3)$$

Momentum transport equations:

X-direction: $$U\frac{\partial U}{\partial X}+V\frac{\partial U}{\partial Y}=-\frac{\partial P}{\partial X}+Pr\left(1+\frac{1}{\eta}\right)\left[\frac{\partial^2 U}{\partial X^2}+\frac{\partial^2 U}{\partial Y^2}\right] \qquad (4)$$

Y-direction: $$U\frac{\partial V}{\partial X}+V\frac{\partial V}{\partial Y}=-\frac{\partial P}{\partial Y}+Pr\left(1+\frac{1}{\eta}\right)\left[\frac{\partial^2 V}{\partial X^2}+\frac{\partial^2 V}{\partial Y^2}\right]+RaPr\varphi \qquad (5)$$

Energy transport equation:

$$U\frac{\partial \varphi}{\partial X}+V\frac{\partial \varphi}{\partial Y}=\frac{\partial^2 \varphi}{\partial X^2}+\frac{\partial^2 \varphi}{\partial Y^2} \qquad (6)$$

The non-dimensional governing equations were derived from the original equations with the aid of the following parameters[48]:

$$\left(X,Y\right)=\frac{\left(x,y\right)}{L},\ AR=\frac{W}{L},U=\frac{uL}{\alpha},V=\frac{vL}{\alpha},\varphi=\frac{T-T_c}{T_h-T_c},P=\frac{pL^2}{\rho\alpha^2},Ra=\frac{g\beta\left(T_h-T_c\right)L^3}{\alpha v}Pr=\frac{\upsilon}{\alpha} \qquad (7)$$

The boundary conditions of flow are prescribed on all the solid walls as $U=V=0$, while the isothermal conditions are set along the boundaries of the enclosure as $\varphi_c=0$ and the walls of the heated rectangular cylinder are maintained at a temperature $\varphi_h=1.0$.

2.2 Solution techniques

The computational fluid dynamics method employed in the present study leverages the finite element formulation method. The Boolean operation was used to produce the region occupied by Casson fluid; furthermore, Casson fluid was added to the model as working fluid. The walls of the model were then subjected to the prevailing boundary conditions. The mesh of the domain employed for computation was produced by using the extremely fine grid size (see Figure 2) and the free triangular mesh options in COMSOL Multiphysics 5.6. software. The dimensionless equations governing the study were then implemented within the

COMSOL Multiphysics environment, while the criterion for convergence was specified as 10^{-6}.

The heat transfer along the walls is reckoned by following [49–51]: therefore, the local and mean Nusselt numbers are cast respectively as:

$$Nu_L = -\frac{\partial \varphi}{\partial n} \tag{8}$$

$$\overline{Nu} = \frac{1}{4L}\int_0^{4L} Nu_L \, dL \tag{9}$$

2.3 Computation of the stream function

The flow field within the annulus is depicted by streamlines, which are derived from the velocity components (U and V) as follows[52]:

$$U = \frac{\partial \psi}{\partial Y}, \qquad V = -\frac{\partial \psi}{\partial X} \tag{10}$$

The stream function equation, which is a consequence of the relationship between the velocity components of the two-dimensional flow is as expressed in equation (11)[53]:

$$\frac{\partial^2 \psi}{\partial X^2} + \frac{\partial^2 \psi}{\partial Y^2} = \frac{\partial U}{\partial Y} - \frac{\partial V}{\partial X} \tag{11}$$

The boundary condition of Eq. (11) is that $\psi = 0$ along the solid boundaries.

3. Results and discussion

3.1 Result validation

The numerical code used for the current investigation is validated by comparing the results of average Nusselt number obtained on the hot wall from the current investigation (see Figure 3a) in the absence of the obstruction with those presented in Figure 3b as obtained by [35] under the same thermal boundary conditions for the same range of Casson fluid parameter $(0.1 \le \eta \le 1.0)$ and Rayleigh number $(10^2 \le Ra \le 10^6)$. The Comparison shows that the current work aligns well with the results of [35]. Furthermore, to validate the quality of the mesh used for the present study, grid sensitivity tests based on average Nusselt number were conducted for various mesh sizes and the results are presented in Table 1. The results confirms that the solution is independent of mesh for the case of the extremely fine grid size.

3.2 Isotherms and stream function plots

Figure 4 shows the plot of isotherms and stream functions for $AR = 0.3$, $\gamma = 0^{\circ}$ and $\eta = 1.0$. For $Ra = 10^3$, and $Ra = 10^4$, the isotherms were observed to be almost parallel to the enclosure walls; this observation is due to the fact that the dominant mode of heat transfer in these regimes is conduction. When $Ra = 10^5$, the isothermal lines around the enclosure and cylinder walls had deviated from being parallel to the walls and plumes were observed to have been formed above the inner cylinder and the isotherms are dense around the inner cylinder and spaced outwardly. These features signify that the dominant mode of heat transport is no longer by conduction but by convection, and the heat transfer was noticed to have been enhanced. When $Ra = 10^6$, the spacing between the isotherms increased except at the left and right sides of the enclosure and around the cylinder where they are very dense; also, the plume formed above the cylinder is more pronounced compared to that formed when $Ra = 10^5$. The trend observed underscores the fact that convection mode of heat transfer had become much more vigorous than when $Ra = 10^5$, thus giving rise to higher heat transfer augmentation.

For the stream functions, at $Ra = 10^3$, the streamlines to the right of the cylinder rotate in a clockwise fashion while those to the left of the cylinder rotate in an anticlockwise manner. These circulation patterns are consistent with the thermal conditions of the walls where the fluid around the heated cylinder is expected to be heated up and consequently displaced by cold fluid. The flow around the cylinder is symmetric around it thus giving rise to two secondary vortices on both the left and right sides of the inner rectangular cylinder. When $Ra = 10^4$, the circulation patterns were sustained with improved strength of the vortices at the cores of the primary circulations and a vortex disappeared on each side of the cylinder as the stream functions became less dense. Meanwhile, when $Ra = 10^5$, the stream functions became closely packed towards the top with an improvement in the flow strength around the top portion of the enclosure. When $Ra = 10^6$, the streamlines widened and become denser towards the upper part of the enclosure and also, the strength of the secondary circulations and the general flow pattern around the top portion of the enclosure had improved significantly compared to when $Ra = 10^5$.

Figure 5 displays the effects of Rayleigh number (Ra) on isotherm (left) and stream function (right) when $AR = 0.3$, $\gamma = 90^\circ$ and $\eta = 1.0$. At $Ra = 10^3$, the isotherms are evenly spaced and distributed around the enclosure but became dense towards the inner rectangular cylinder as heat transfer rate increased inwards. When $Ra = 10^4$, the isotherms began drifting towards the upper part of the enclosure and they formed plumes at $Ra = 10^5$. From $Ra = 10^4$ to $Ra = 10^5$, the isotherms became spaced out with increased density towards the top of the enclosure and highest around the inner rectangle cylinder. Furthermore, comparing isothermal plots in Figure 4 with those in Figure 5, which corresponds to increasing inclination angle of the cylinder from $\gamma = 0^\circ$ to $\gamma = 90^\circ$, it can be observed that the heat transfer strength above the cylinder for the case of $\gamma = 0^\circ$ is more than that for $\gamma = 90^\circ$, this is particularly evident for $Ra = 10^5$ and $Ra = 10^6$ where the plumes above the cylinder which indicate convection mode of heat transfer above the cylinder is more pronounced for $\gamma = 0^\circ$ than for $\gamma = 90^\circ$; this behaviour is due to larger surface area available at the top of the cylinder for $\gamma = 0^\circ$ when compared with the cylinder top for $\gamma = 90^\circ$. For the stream functions, the pattern of rotation of the circulations are the same as those in Figure 4. Additionally, as revealed by the maximum stream function values, as Ra value increases, the strength of flow when $\gamma = 90^\circ$ increased more compared to when $\gamma = 0^\circ$; the reason for the higher strength in the flow observed when the cylinder is positioned vertically ($\gamma = 90^\circ$) is that the effect of gravity on the cylinder in the vertical position is more than when it is in the horizontal position ($\gamma = 0^\circ$ *).*

Figure 6 presents the influence of Casson fluid parameter (η) on isotherm (left) and stream function (right) when $AR = 0.7$, $Ra = 10^6$ and $\gamma = 0^0$. When $\eta = 0.1$, the isotherms formed plumes above the rectangular cylinder and the isothermal lines are dense around the cylinder and close to the enclosure top. As Casson fluid parameter increases from $\eta = 0.3$ to $\eta = 1.0$, the isotherms become more spaced out around the top portion of the cylinder with the plume becoming more pronounced with increasing Casson fluid parameter. This is an indication that increasing Casson fluid parameter results in the improvement in convective strength which indicates enhancements in heat transfer. For the range of Casson fluid parameters considered, the stream function plots to the right of the cylinder rotate clockwise while those to the left of the cylinder rotate anticlockwise; also, the streamline strengthen is intensified with improvement in the Casson fluid parameter which is revealed by the progressive increase in the maximum stream function value as the Casson fluid parameter rises; this is an indication that Casson fluid parameter increase enhances the fluid flow strength. These observations are because as the Casson fluid parameter increases, the viscosity of the fluid diminishes therefore higher fluid velocity is realized for higher Casson fluid parameter. Additionally, the stream function plot when $\eta = 0.1$ features two secondary vortices at the bottom portion of the enclosure while the stream function at the upper part is closely packed unlike the lower part of the enclosure. As η increases from 0.3 to 1.0, the two vortices below the inner cylinder disappeared and the stream function becomes progressively more closely parked at the upper part of the enclosure which is also an indication that the rate of heat transfer increases steadily with improvement in Casson fluid parameter.

Figure 7 shows the influence of Casson fluid parameter (η) on isotherm (left) and stream function (right) when $AR = 0.7$, $Ra = 10^6$ and $\gamma = 90^\circ$. Comparing the isotherms in Figure 6 with those in Figure 7 reveals that the plumes above the cylinder for the range of Casson fluid parameters considered when $\gamma = 0^\circ$ are more pronounced than those formed when $\gamma = 90^\circ$ this shows that heat transfer augmentation appears to be more favoured when the cylinder is in the horizontal position than in the vertical position. Similarly, the flow strength improves more when the cylinder is in a vertical position than when in a horizontal position, this revelation is evident in the maximum stream function values as Casson fluid parameter improves and this observation is consistent with the fact that the fluid is able to fall more freely under gravity when the cylinder is in a vertical position than in the horizontal position.

Figure 8 displays the implication of inclination angle variation on isotherm (left) and stream function (right) for $\eta = 1.0$, $Ra = 10^6$ and $AR = 0.7$. When $\gamma = 0^\circ$, the isothermal lines are symmetrical about the center of the cylinder and the plumes formed spread out towards the upper portion of the enclosure. As the cylinder inclination angle increases, the plumes were observed to skew toward the direction of tilt of the cylinder and the isothermal lines are symmetrical about the cylinder when $\gamma = 90^\circ$ which is an indication that an equal rate of heat transfer occurred on both the left and right sides of the cylinder. For all the inclination angles considered for the stream function plots, the circulations to the right of the cylinder rotate clockwise while the ones to the left of the cylinder rotate anticlockwise. When $\gamma = 0^\circ$, the stream functions are closely and evenly packed above the cylinder; between $\gamma = 30^\circ$ and $\gamma = 60^\circ$, the stream functions deformed to conform with the orientation of the cylinder and when $\gamma = 90^\circ$, the stream functions became symmetric about the cylinder. Furthermore, the flow strength increases as the cylinder inclination angle was increased from $\gamma = 0^\circ$ to $\gamma = 30^\circ$, this increase is evident in the stream function values where the maximum stream function value increased correspondingly from 19 (when $\gamma = 0^\circ$) to 23 (when $\gamma = 30^\circ$), when the inclination angle was increased further to $\gamma = 45^\circ$, the maximum flow strength was sustained, but at $\gamma = 60^\circ$ and beyond, the maximum flow strength declined. This trend in the decrease in the flow strength for cylinder angles beyond $\gamma = 45^\circ$ could be due to a reduction in the strength of the buoyancy force and therefore not able to push the fluid with higher force over the cylinder.

Figure 9 presents the effects of aspect ratio on isotherm (left) and stream function (right) plots when $\eta = 1.0$, $Ra = 10^6$ and $\gamma = 0^\circ$. When $AR = 0.1$, plumes were seen to be formed, and as AR value increases, the plumes spread more outward toward the upper portion of the enclosure and isothermal lines close to the vertical walls of the enclosure were observed to deviate the more from being vertical which is an indication that with improvements in AR value, more heat transfer enhancement along the vertical walls of the enclosure occurred. This is because as the heated cylinder wall gets closer to the cold vertical walls, the temperature difference between the vertical enclosure walls and the adjacent fluid become steeper and this favours more heat transport. However, for the cylinder, as AR expands, the isothermal lines become more closely packed and the temperature values from one isothermal lines to another becomes very close thus the difference in the temperature value from one isotherm to the other becomes smaller and smaller thus leading to declined heat transfer from the cylinder wall as AR grows in value. For the stream function, the flow began to be restricted largely to the upper portion of the cylinder possibly due to the reduction in the size of the flow passage between the enclosure wall and the cylinder walls. In addition, the maximum flow strength when $AR = 0.1$ is 18 and it remained constant till $AR = 0.5$ when $\Psi_{max} = 19.0$ and thereafter remained unchanged.

3.3 Average Nusselt number

Figures 10 and 11 present the plots of the average Nusselt number $\overline{Nu}$ of the heated cylinder walls against cylinder inclination angle for the various Rayleigh numbers considered when $\eta = 1.0$, $AR = 0.1$ and 0.7. Both plots show that the average Nusselt number of the cylinder walls increase with increasing Rayleigh number which is due to the increase in buoyancy force. For $AR = 0.1$, the influence of cylinder inclination angle on the cylinder wall is negligible particularly for Rayleigh number in the range of $10^3 \leq Ra \leq 10^5$, which implies that the effect of buoyance force outweighs the impact of inclination angle on the heat transport. And for $Ra = 10^6$, the average Nusselt number improves marginally for inclination angle in the interval of $0^\circ \leq \gamma \leq 45^\circ$. Beyond $\gamma > 45^\circ$, inclination angle improvement resulted in average Nusselt number reduction. This trend is justified by the isothermal contour plots in Figure 8 in which $0^\circ \leq \gamma \leq 45^\circ$, the intensity of the plumes' colour increased and then decreased beyond $\gamma = 45^\circ$. When AR is increased to *0.7* as presented in Figure 11, for *Ra* in the interval of $10^3 \leq Ra \leq 10^4$, and cylinder inclination angle of $0^\circ \leq \gamma \leq 45^\circ$, the average Nusselt number is insensitive to cylinder orientation possibly because the effect of buoyancy force on heat transfer is more pronounced than the impact of cylinder orientation. While for $Ra = 10^5$ inclination angle beyond $\gamma > 45^\circ$ improved heat transfer of the cylinder, and for $Ra = 10^6$, the average Nusselt number increases with inclination angle.

Figures 12 and 13 represent the plots of the average Nusselt number of the enclosure walls against cylinder orientation angle for the various Rayleigh numbers considered. For the case of $AR = 0.1$ which is depicted in Figure 12, the amount of heat transferred when the cylinder is oriented vertically is the same as that transferred when the cylinder is in a horizontal position. For all the Rayleigh numbers considered, the influence of cylinder orientation angle on heat transfer is nearly inconsequential especially for Rayleigh number in the interval of $10^3 \le Ra \le 10^5$; which implies that the effect of heating overrides the impact of inclination in these flow regimes. While for $Ra = 10^6$, and $0^\circ \le \gamma \le 45^\circ$, the average Nusselt number improves marginally and then reduces beyond $\gamma > 45^\circ$. Figure 13 corresponds to increasing the aspect ratio of Figure 12 to $AR = 0.7$, as opposed to the heated cylinder wall, increase in AR for the enclosure wall resulted in heat transfer enhancement; this is due to the fact that as the cylinder increases in size, the fluid adjacent to the enclosure wall get heated up thus resulting in a steep gradient between the cold enclosure walls and the hot adjacent fluid, this therefore accounts for the trend observed. For Ra and γ in the intervals of Ra $10^3 \le Ra \le 10^4$, and $0^\circ \le \gamma \le 45^\circ$ increase in inclination angle marginally reduces the Nu value of the enclosure but beyond $\gamma > 45^\circ$, inclination angle improvement resulted in the average Nusselt increment. For $Ra = 10^5$, there exists a local minimum Nusselt number at $\gamma = 30^\circ$ and further increase in γ results in gradual improvement in $\overline{Nu}$ value. While for $Ra = 10^6$, and for all the inclination angles considered, *Nuav* improved with improvement in inclination angle.

Figures 14 and 15 represent the impact of Casson fluid parameter on the average Nusselt number of the heated cylinder walls for various Rayleigh numbers when $AR = 0.1$ and the cylinder is oriented horizontally. Both Figures 14 and 15 show that Casson fluid parameter results in heat transfer augmentation particularly for Ra in the interval of $10^5 \le Ra \le 10^6$. Furthermore, consistent with earlier observation, AR improvement results in heat transfer inhibition. Figures 16 and 17 show the implication of Casson fluid parameter on the heat transfer profile of the enclosure walls for $AR = 0.1$ and $AR = 0.7$. The plots show that Casson fluid Parameter improved heat transfer rate and the improvement became more evident for Ra in the range of $10^5 \le Ra \le 10^6$. The impact of Casson fluid parameter (η) on heat transfer is such that as η increases, the effective viscosity of the fluid decreases, furthermore, the thickness of the boundary layer also decreases (see the plumes in Figure 7) which translates to increase in the temperature gradient of the wall and by extension results in improved heat transfer rate. Figures 18 and 19 are the charts for the responses of the average Nusselt number to aspect ratio variations along the cylinder walls for $\gamma = 0^{\circ}$ and $\gamma = 90^{\circ}$ when Casson fluid parameter $\eta = 1.0$. Both plots show that heat transfer enhancement is discouraged with improvement in AR value; this observation is consistent with that in Figure 9. Furthermore, when $\gamma = 90^{\circ}$ the heat transfer was enhanced noticeably for Ra values of $10^5 \le Ra \le 10^6$. Figures 20 and 21 present the influence of AR on average Nusselt number on the enclosure walls for $\gamma = 0^{\circ}$ and $\gamma = 90^{\circ}$ when Casson fluid parameter $\eta = 1.0$. For both plots in Figures 20 and 21, AR improvement supports heat transfer augmentation. The physical explanation for the observed trend is as enunciated in Figure 9. Additionally, the vertical orientation of the cylinder augmented heat transfer more than the horizontal position of the cylinder particularly for Ra range of $10^5 \le Ra \le 10^6$. For Ra in the range of $10^3 \le Ra \le 10^4$, aligning the cylinder in the vertical position does not result in a tangible improvement in heat transfer augmentation.

4. Conclusions

This research article presents the flow and convective heat transfer of Casson fluid around a rectangular cylinder located concentrically inside a cold square enclosure. The problem was solved numerically, and the results obtained led to the following conclusions.

1. Casson fluid parameter improvement has no significant impact on the average Nusselt numbers of both the cylinder and enclosure walls for Rayleigh number in the range of $10^3 \le Ra \le 10^4$, but beyond $Ra = 10^4$ increase in the Casson fluid parameter resulted in heat transfer augmentation for both the cylinder and enclosure walls.

2. For both the horizontal and vertical positions of the cylinder, the streamline intensity rises as the Casson fluid parameter rises; however, the streamline strength for the cylinder in vertical position gave rise to higher streamline strength.
3. The average Nusselt number of the enclosure increases as the aspect ratio increases, but for the cylinder, the average Nusselt number decreases with increase in aspect ratio of the cylinder.
4. The streamlines are symmetric about the cylinder for all the aspect ratios considered and the highest streamline strength $(\Psi_{max} = 19.0)$ occurred when $AR = 0.5$.
5. For the range of Casson fluid parameter, aspect ratio, and inclination angle considered for both the cylinder and enclosure walls, increasing Ra in the range of $10^3 \le Ra \le 10^4$ resulted in marginal improvements in the heat transferred but increasing Ra beyond 10^4 resulted in significant improvement in heat transfer which was due to improvement in convective transport.
6. The impact of inclination angle for both the enclosure and cylinder walls for the smallest aspect ratio ($AR = 0.1$) considered is inconsequential for Rayleigh number in the range of $10^3 \le Ra \le 10^4$; while for Rayleigh number $Ra > 10^4$, the maximum heat transfer occurred at $\gamma = 45^\circ$.
7. The implication of inclination angle for both the enclosure and cylinder walls for the largest aspect ratio considered ($AR = 0.7$) reveals that for Ra in the interval of $10^3 \le Ra \le 10^4$, and cylinder inclination angle of $0^\circ \le \gamma \le 45^\circ$, the average Nusselt number reduces with increasing inclination angle; and for $\gamma < 45^\circ$, γ increment augmented heat transfer. While for $Ra = 10^5$, inclination angle beyond $\gamma > 30^\circ$ improved heat transfer of the cylinder and enclosure walls. For $Ra = 10^6$, the average Nusselt numbers of the walls of both the cylinder and enclosure increase with inclination angle.

DECLARATION

Consent for Publication

The authors gave their consent for the publication of the manuscript.

Informed consent

Not applicable

Acknowledgment

Not applicable

Authors' contributions

O.A. Olayemi supervised the numerical experiment conducted. T.F. Ajide, A.M. Obalalu, and M.A. Ismael planned the project implementation. T.F. Ajide, AM. Obalalu, and M.A. Ismael analyzed the results of the investigation. T.F. Ajide and AM. Obalalu reported the results while O. A. Olayemi and M.A. Ismael reviewed the manuscript. All the authors actively contributed to the scientific discussion and approved the final version of the manuscript.

Funding statement

The research did not receive any financial support.

Data availability statement

The data for the present investigation are available in the article.

Code available Not applicable

Disclosure statement

The authors have no relevant financial and non-financial interests to disclose.

REFERENCES

1. Animasaun, I.L., Adebile, E.A., and Fagbade, A. I. "Casson fluid flow with variable thermo-physical property along exponentially stretching sheet with suction and exponentially decaying internal heat generation using the homotopy analysis method, " *J. Niger. Math. Soc.*, **35**(1), pp. 1–17 (2016). DOI:10.1016/j.jnnms.2015.02.001

2. Das, D., Roy, M., and Basak, T. " Studies on natural convection within enclosures of various (non-square) shapes – A review," *Int. J. Heat Mass Transf.,* **106**, pp. 356–406 (2017). DOI: 10.1016/j.ijheatmasstransfer.2016.08.034

3. Baïri, A., Zarco-Pernia, E., García De María, JM. "A review on natural convection in enclosures for engineering applications. the particular case of the parallelogrammic diode cavity," *Appl. Therm. Eng*., **63**, pp. 304–322 (2014) DOI: 10.1016/j.applthermaleng.2013.10.065

4. Assad, Mamdouh, and Marc A. Rosen, eds. "Design and performance optimization of renewable energy systems", *Academic Press*, 2021.

5. Rostami, S., Aghakhani, S., Pordanjani, A. H. et al. "A review on the control parameters of natural convection in different shaped cavities with and without nanofluid, "*Processes* **8**(9), pp. 1011 (2020). DOI: 10.3390/pr8091011

6. Olayemi, O. A., Khaled, A. F., Temitope, O. J. et al. "Parametric study of natural convection heat transfer from an inclined rectangular cylinder embedded in a square enclosure", *Aust. J. Mech. Eng*., **21**(2), pp. 668–681 (2023), DOI:10.1080/14484846.2021.1913853

7. Bhukya, L. and Nandiraju, S. "A novel photovoltaic maximum power point tracking technique based on grasshopper optimized fuzzy logic approach" *Int. J. Hydrogen Energy*., **45**(16), pp. 9416–9427 (2020). DOI: 10.1016/j.ijhydene.2020.01.219

8. Aghighi, M. S., Metivier, C., and Masoumi, H. "Natural convection of Casson fluid in a square enclosure," *Multidiscip Model Mater Struct.*, **16**(5), pp. 1245–1259 (2020). DOI: 10.1108/MMMS-11-2019-0192

9. Pop, I. and Sheremet, M. "Free convection in a square cavity filled with a Casson fluid under the effects of thermal radiation and viscous dissipation", *Int. J. Numer. Methods. Heat Fluid Flow*, 27(10):2318–2332 (2017). DOI: 10.1108/HFF-09-2016-0352

10. Hirpho, M. "Mixed convection of Casson fluid in a differentially heated bottom wavy wall", *Heliyon* **7**(6), pp. e07361 (2021). DOI: 10.1016/j.heliyon.2021.e07361

11. Ghalambaz, M., Sabour, M., Pop, I., Wen, D. " Free convection heat transfer of MgO-MWCNTs/EG hybrid nanofluid in a porous complex shaped cavity with MHD and thermal radiation effects", *Int J Numer Methods Heat Fluid Flow.*, **29**(11), pp. 4349–4376 (2019) DOI:10.1108/HFF-04-2019-0339

12. Alzahrani, A. K., Sivanandam Sivasankaran, and M. Bhuvaneswari. "Numerical Simulation on Convection and Thermal Radiation of Casson Fluid in an Enclosure with Entropy Generation", *Entropy*., **22**(2), pp. 229, (2020). DOI:10.3390/e22020229

13. Olayemi, OA., Obalalu, AM., Odetunde, CB., et al. "Heat transfer enhancement of magnetized nanofluid flow due to a stretchable rotating disk with variable thermophysical properties effects", Eur. *Phys. J. Plus.*, **137**(3), pp. 393 (2022). DOI:10.1140/epjp/s13360-022-02579-w

14. Trisaksri, V. and Wongwises, S. "Critical review of heat transfer characteristics of nanofluids", *Renew Sustain Energy Rev*., **11**(3), pp. 512–523 (2007). DOI:1 0.1016/j.rser.2005.01.010

15. Olayemi, O. A., Al- Farhany, K., Obalalu, A. M. et al., "Magnetoconvection around an elliptic cylinder placed in a lid- driven square enclosure subjected to internal heat generation or absorption", *Heat Transf.*, **51**(6), pp. 4950–4976 (2022). DOI: 10.1002/htj.22530

16. Olayemi, O. A., Salaudeen, A., and Al-farhany, K. "Modelling of heat transfer characteristics around a cylindrical-barrier", *Int. J. Eng. Model.*, **35**(1), pp. 83–106 (2022). DOI:10.31534/engmod.2022.ri.05b

17. Ali, M.M., Akhter, R., and Alim, M. A. "Performance of flow and heat transfer analysis of mixed convection in Casson fluid filled lid driven cavity including solid obstacle with magnetic impact", *SN. Appl. Sci.*, **3**, pp. 1-5 (2021). DOI: 10.1007/s42452-021-04243-x

18. Ghigo, A. R., Lagrée, P. Y., and Fullana, J. M. "A time-dependent non-Newtonian extension of a 1D blood flow model", *J. Nonnewton Fluid Mech.*, **253**, pp. 36–49 (2018). DOI: 10.1016/j.jnnfm.2018.01.004

19. Aneja, M., Chandra, A., and Sharma, S. "Natural convection in a partially heated porous cavity to Casson fluid", *Int. Commun. Heat Mass Transf.*, **114**, pp. 104555 (2020). DOI: 10.1016/j.icheatmasstransfer.2020.104555

20. Rehman, K.U., Malik, A. A., Malik, M.Y., et al. "Numerical study of double stratification in Casson fluid flow in the presence of mixed convection and chemical reaction", *Results Phys*., 7, pp. 2997–3006 (2017). DOI: 10.1016/j.rinp.2017.08.020

21. Hamid, M., Usman, M., Khan, Z. H., et al." Dual solutions and stability analysis of flow and heat transfer of Casson fluid over a stretching sheet", *Phys. Lett. Sect A Gen At Solid State Phys*., **383**(20), pp. 2400–2408 (2019)**.** DOI: 10.1016/j.physleta.2019.04.050.

22. Obalalu, A., Olayemi, O., and Odetunde, C. "Significance of Thermophoresis and Brownian Motion on a Reactive Casson-Williamson Nanofluid Past a Vertical Moving Cylinder", *Comput. Therm. Sci. An. Int. J.* **15**(1), pp. 75–91 (2022) DOI:10.1615/computthermalscien.2022041799.

23. Papanastasiou, T. C. and Boudouvis, A. G. "Flows of viscoplastic materials: Models and computations", *Comput Struct*, **64**(1-4), pp. 677–694 (1997). DOI:10.1016/S0045-7949(96)00167-8

24. Chhabra, Raj P., and John Francis Richardson. *Non-Newtonian flow and applied rheology: engineering applications*. Butterworth-Heinemann, 2011.

25. Mittal, A. S. and Patel, H. R. "Influence of thermophoresis and Brownian motion on mixed convection two dimensional MHD Casson fluid flow with non-linear radiation and

heat generation", *Phys. A. Stat. Mech. its Appl.*, **537**, pp. 122710 (2020). DOI: 10.1016/j.physa.2019.122710

26. Rehman, K. U., Malik, M. Y., Al-Mdallal, Q. M., et al. " Heat transfer analysis on buoyantly convective non-Newtonian stream in a hexagonal enclosure rooted with T-Shaped flipper: hybrid meshed analysis", *Case Stud. Therm. Eng.*, **21**, pp. 100725 (2020). DOI: 10.1016/j.csite.2020.100725

27. Sivasankaran, S., Bhuvaneswari, M., and Alzahrani, A. K. "Numerical simulation on convection of non-Newtonian fluid in a porous enclosure with non-uniform heating and thermal radiation", *Alexandria Eng. J.*, **59**(5), pp. 3315–3323 (2020) DOI: 10.1016/j.aej.2020.04.045

28. Lam, P.A.K., and Prakash, K.A. "Effect of magnetic field on natural convection and entropy generation in Al2O3/water nanofluid filled enclosure with twin protruding heat sources", *J. Therm. Sci. Eng*. Appl., **9**(2), pp. 024502 (2017). DOI: 10.1115/1.4035810

29. Das, S., Mondal, H., Kundu, P. K., et al. "Spectral quasi-linearization method for Casson fluid with homogeneous heterogeneous reaction in presence of nonlinear thermal radiation over an exponential stretching sheet," *Multidiscip Model Mater Struct*., **15**(2), pp. 398–417 (2019) DOI:10.1108/MMMS-04-2018-0073

30. Kumaran, G. and Sandeep, N. "Thermophoresis and Brownian moment effects on parabolic flow of MHD Casson and Williamson fluids with cross diffusion", *J. Mol. Liq*., **233**, pp. 262–269 (2017). DOI: 10.1016/j.molliq.2017.03.031.

31. Mahanthesh, B., Brizlyn, T., Shehzad, S. A., et al. "Nonlinear thermo-solutal convective flow of Casson fluid over an oscillating plate due to non-coaxial rotation with quadratic density fluctuation: Exact solutions", *Multidiscip. Model. Mater. Struct.* **15**(4), pp. 818–842 (2019). DOI:10.1108/MMMS-06-2018-0124.

32. Kumar, A., Sugunamma, V., and Sandeep, N. "Impact of Non-linear Radiation on MHD Non-aligned Stagnation Point Flow of Micropolar Fluid over a Convective Surface", *J. Non-Equilibrium Thermodyn.*, **4**3(4), pp. 327–345 (2018). DOI:10.1515/jnet-2018-0022.

33. Raju, C. S. K., Sandeep, N., Sugunamma, V., et al. "Heat and mass transfer in magnetohydrodynamic Casson fluid over an exponentially permeable stretching surface", *Eng. Sci. Technol. an Int. J.*, **19**(1), pp. 45–52 (2016). DOI: 10.1016/j.jestch.2015.05.010

34. Hamid, M., Usman, M., Khan, Z. H., et al. "Heat transfer and flow analysis of Casson fluid enclosed in a partially heated trapezoidal cavity", *Int. Commun. Heat Mass Transf.*, **108**, p. 104284 (2019). DOI:10.1016/j.icheatmasstransfer.2019.104284.

35. Devi, T. S., Lakshmi, C. V., Venkatadri, K., et al. " Simulation of unsteady natural convection flow of a casson viscoplastic fluid in a square enclosure utilizing a mac algorithm," *Heat Transf.*, **49**(4), pp. 1769–1787 (2020). DOI:10.1002/htj.21690.

36. Pasha, P., Mirzaei, S., and Zarinfar, M. "Application of numerical methods in micropolar fluid flow and heat transfer in permeable plates," *Alexandria Eng. J.*, **61**(4), pp. 2663–2672 (2022). DOI:10.1016/j.aej.2021.08.040

37. Pasha, P., Nabi, H., Peiravi, M. M., et al. "Hybrid Investigation of Thermal Conductivity and Viscosity Changeable With Generation/Absorption Heat Source", *Comput. Therm. Sci.*, **14(1)**, pp.19–30 (2022). DOI:10.1615/ComputThermalScien.2021039390

38. Abdollahzadeh, M. J., Fathollahi, R., Pasha, P., et al. "Surveying the hybrid of radiation and magnetic parameters on Maxwell liquid with TiO2 nanotube influence of different blades," *Heat Transf.*, **51(6)**, pp. 4858–4881 (2022). DOI:10.1002/htj.22526

39. Fathollahi, R., Hesaraki, S., Bostani, A., et al. "Applying numerical and computational methods to investigate the changes in the fluid parameters of the fluid passing over fins of different shapes with the finite element method", *Int. J. Thermofluids.*, **15**, pp. 100187 (2022). DOI:10.1016/j.ijft.2022.100187.

40. Fatehinasab, R., Shafiee, H., Afshari, M., et al. "Hybrid surveying of radiation and magnetic impacts on Maxwell fluid with MWCNT nanotube influence of two wire loops", *ZAMM Z. fur. Angew. Math. Mech.*, **103**(1), pp. p.e202200186 (2022). DOI:10.1002/zamm.202200186

41. Vishnu Ganesh, N., Al-Mdallal Q. M., Öztop H. F., et al. "Analysis of natural convection for a Casson-based multiwall carbon nanotube nanofluid in a partially heated wavy enclosure with a circular obstacle in the presence of thermal radiation", *J. Adv. Res.*, **39**, pp. 167–185 (2022). DOI:10.1016/j.jare.2021.10.006.

42. Selimefendigil, F. and Öztop, H. F. "Thermal management for conjugate heat transfer of curved solid conductive panel coupled with different cooling systems using non-Newtonian power law nanofluid applicable to photovoltaic panel systems", *Int. J. Therm. Sci.*, **173**, p. 107390 (2022). DOI:10.1016/j.ijthermalsci.2021.107390.

43. Fares, R., Mebarek-Oudina, F., Aissa, A., et al. "Optimal entropy generation in Darcy-Forchheimer magnetized flow in a square enclosure filled with silver based water nanoliquid", *J. Therm. Anal Calorim*, **147**, pp. 1571–1581 (2022). DOI:10.1007/s10973-020-10518-z.

44. Hafeez, M. B., Krawczuk, M., and Nisar, K. S., et al. "A finite element analysis of thermal energy inclination based on ternary hybrid nanoparticles influenced by induced magnetic field", *Int. Commun. Heat Mass Transf.*, **135,** pp. 106074 (2022). DOI:10.1016/j.icheatmasstransfer.2022.106074.

45. Hafeez, M. B., Khan, M. S., Qureshi, I. H., et al. "Particle rotation effects in Cosserat-Maxwell boundary layer flow with non-Fourier heat transfer using a new novel approach," *Sci. Iran.*, 28(3), pp. 1223–1235 (2021). DOI.org/10.24200/sci.2020.52191.2583.

46. Aghighi, M. S. and Ammar, A. "Aspect ratio effects in Rayleigh-Bénard convection of Herschel-Bulkley fluids", *Eng. Comput.* **34(**5), pp. 1658–1676 (2017). DOI:10.1108/EC-06-2016-0227.

47. Hayat, T., Bilal Ashraf, M., Shehzad, S. A., et al. "Mixed convection flow of casson nanofluid over a stretching sheet with convectively heated chemical reaction and heat source/sink", *J. Appl. Fluid Mech.*, **8(4),** pp. 803–813 (2015). DOI:10.18869/acadpub.jafm.67.223.22995.

48. Olayemi, O. A., Obalalu, A. M., Ibitoye, S. E., et al., "Effects of Geometric Ratios on Heat Transfer in Heated Cylinders: Modelling and Simulation", *Niger. J. Technol. Dev.*, **19**(4), pp. 287–297 (2022). DOI:10.4314/njtd.v19i4.1.

49. Adegun, I. K., Jolayemi, T. S., Olayemi, O. A., et al. "Numerical simulation of forced convective heat transfer in inclined elliptic ducts with multiple internal longitudinal fins," *Alexandria Eng. J.*, **57**(4) (2018). DOI:10.1016/j.aej.2017.01.014.

50. Olayemi, O. A., Ibitoye, S. E., and Obalalu, A. M. "Numerical Analysis of Lid Driven Convective Heat Transfer and Fluid Flow around a Tilted Elliptical Cylinder", Defect *Diffusion Forum.*, **421**, pp. 27–42 (2022). DOI:10.4028/p-lj265m.

51. Adebayo Olayemi, O., Temitope Olabemiwo, J., Osekhoghene Dirisu, J., et al. "Numerical simulation of heat transfer and fluid flow around a cylinder of varying cross-section", *Mater. Today Proc.*, **65**, pp. 2128–2137 (2022). DOI:10.1016/j.matpr.2022.05.010.

52. Olayemi, O. A., Al-Farhany, K., Ibitoye, S.E., et al., "Mixed Convective Heat Transfer in a Lid-Driven Concentric Trapezoidal Enclosure: Numerical Simulation”, Int. *J. Eng. Res. Africa.*, 60, pp. 43–62 (2022). DOI:10.4028/p-kybe41.

53. Olayemi, O. A., Isiaka, M., Al-Farhany, K., et al. "Numerical Analysis of Natural Convection in a Concentric Trapezoidal Enclosure Filled with a Porous Medium," *Int. J. Eng. Res. Africa.*, **61**, pp. 129–150 (2022). DOI:10.4028/p-jza9vq.

Figure 1: Physical Model

Figure 2: Mesh Distribution

Table 1: Presents the mesh independency test of the avarage Nusselt number $\overline{Nu}$ on the enclosure walls for $\eta = 1.0$, $Ra = 10^6$, $\gamma = 90^o$ and $AR = 0.7$.

Figure 3a: $\overline{Nu}$ from the present study versus Ra for various Casson fluid parameter η

Figure 3b: $\overline{Nu}$ versus Ra for various η.

Figure 4: Effect of Ra on isotherm (left) and stream function (right) when $AR = 0.3$, $\gamma = 0^o$ and $\eta = 1.0$

Figure 5: Effects of Rayleigh number (Ra) on isothermlines (left) and stream function (right) at $AR = 0.3$, $\gamma = 90^o$ and $\eta = 1.0$

Figure 6: Influence of Casson fluid parameter η on isotherm (left) and stream function (right) when AR = 0.7, $Ra = 0.6$ and $\gamma = 0^o$

Figure 7: Influence of Casson fluid parameter η on isotherm (left) and stream function (right) when AR = 0.7, $Ra = 0.6$ and $\gamma = 90^o$

Figure 8: Implication of inclination angle variation on isotherms (left) and stream function (right) when $\eta = 1.0$, $Ra = 0.6$ and $AR = 0.1$.

Figure 9: Implication of aspect ratio variation on isotherm (left) and stream function (right) when $\eta = 1.0$, $AR = 0.7$ and $\gamma = 0^o$

Figure 10: $\overline{Nu}$ of the heated cylinder walls against γ for various Ra when $AR = 0.1$ and $\eta = 1.0$

Figure 11: $\overline{Nu}$ of the heated cylinder walls against γ for various Ra when $AR = 0.7$ and $\eta = 1.0$

Figure 12: Variation of $\overline{Nu}$ of enclosure walls versus γ for various Ra when $AR = 0.1$ and $\eta = 1.0$.

Figure 13: Variation of $\overline{Nu}$ of enclosure walls versus γ for various Ra when $AR = 0.7$ and $\eta = 1.0$.

Figure 14: $\overline{Nu}$ of the heated cylinder walls against η for various Ra when $AR = 0.1$ and $\gamma = 0^o$

Figure 15: $\overline{Nu}$ of the heated cylinder walls against η for various Ra when $AR = 0.7$ and $\gamma = 0^o$.

Figure 16: Variation of $\overline{Nu}$ of enclosure walls versus η for various Ra when $AR = 0.1$ and $\gamma = 0^o$

Figure 17: $\overline{Nu}$ of enclosure walls versus η for various Ra when $AR = 0.7$ and $\gamma = 0^o$.

Figure 18: $\overline{Nu}$ of the heated cylinder walls against AR for various Ra when $\eta = 1$ $\gamma = 0^o$.

Figure 19: $\overline{Nu}$ of the heated cylinder walls against AR for various Ra when $\eta = 1$ and $\gamma = 90^o$

Figure 20: $\overline{Nu}$ of enclosure walls versus AR for various Ra when $\eta = 1.0$ and $\gamma = 0^o$.

Figure 21: Variation of $\overline{Nu}$ of enclosure walls versus AR for various Ra when $\eta = 1.0$ and $\gamma = 90^o$

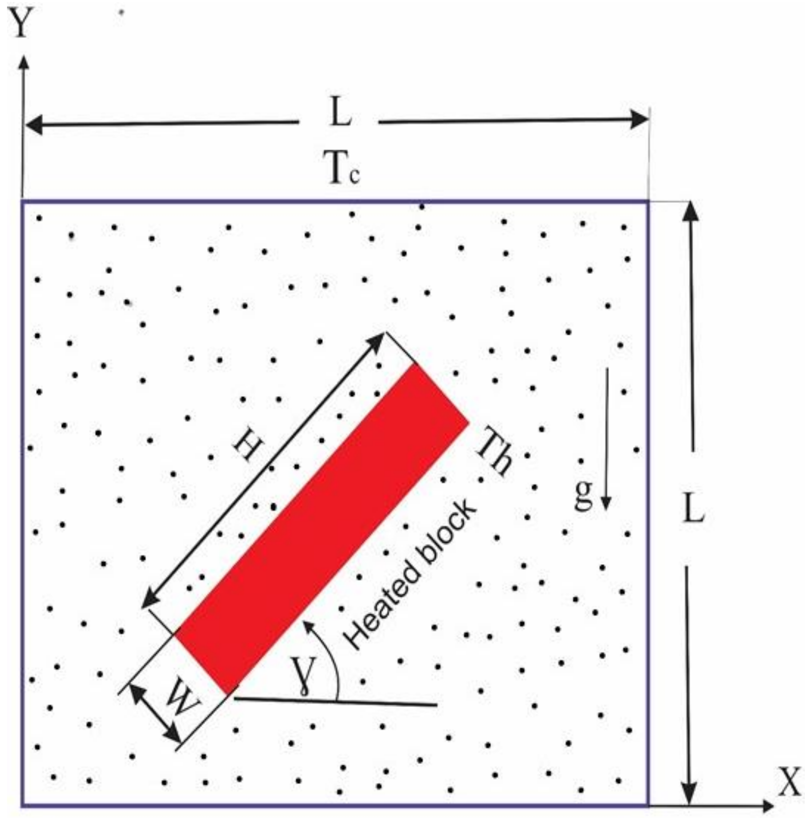

Figure 1

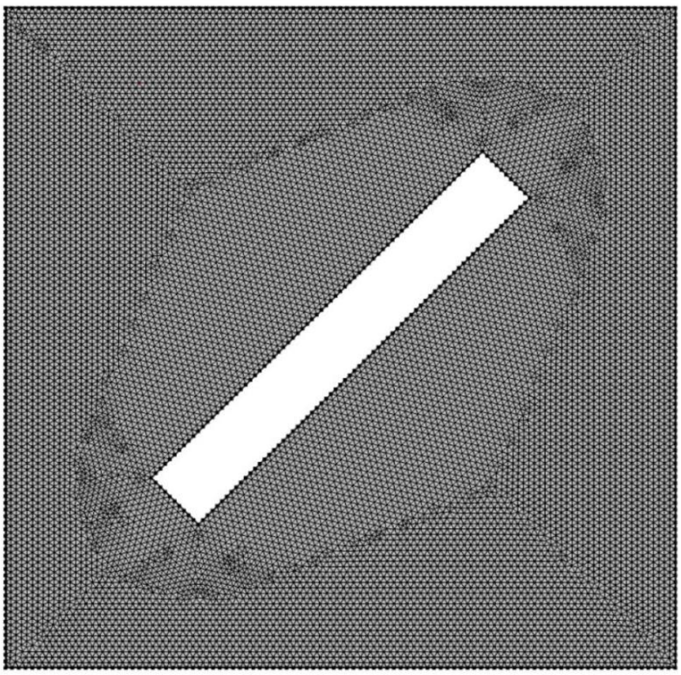

Figure 2

Table 1.0

Size of Mesh	**Mesh elements**	**Average Nusselt number**	**% Absolute Error**
Coarse	3648	5.19	
Normal	4228	4.89	5.78
Fine	4482	4.79	2.04
Finer	5608	4.60	3.97
Extra fine	9152	4.51	1.96
Extremely fine	**23538**	**4.49**	**0.44**

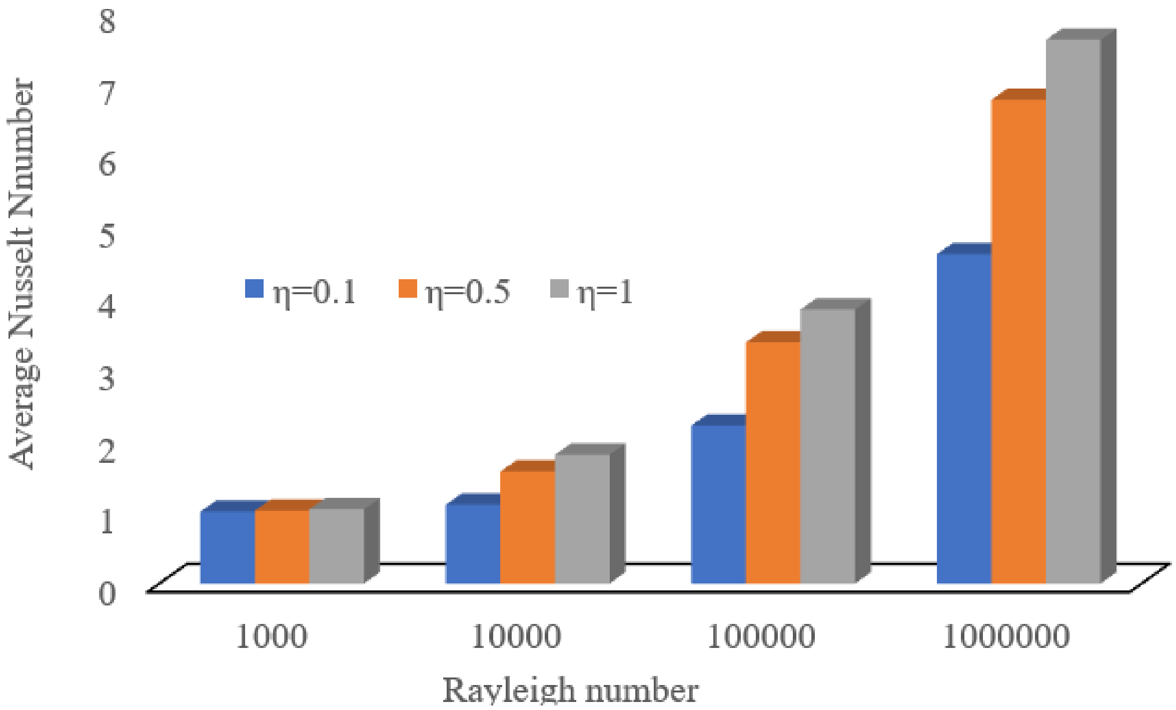

Figure 3a

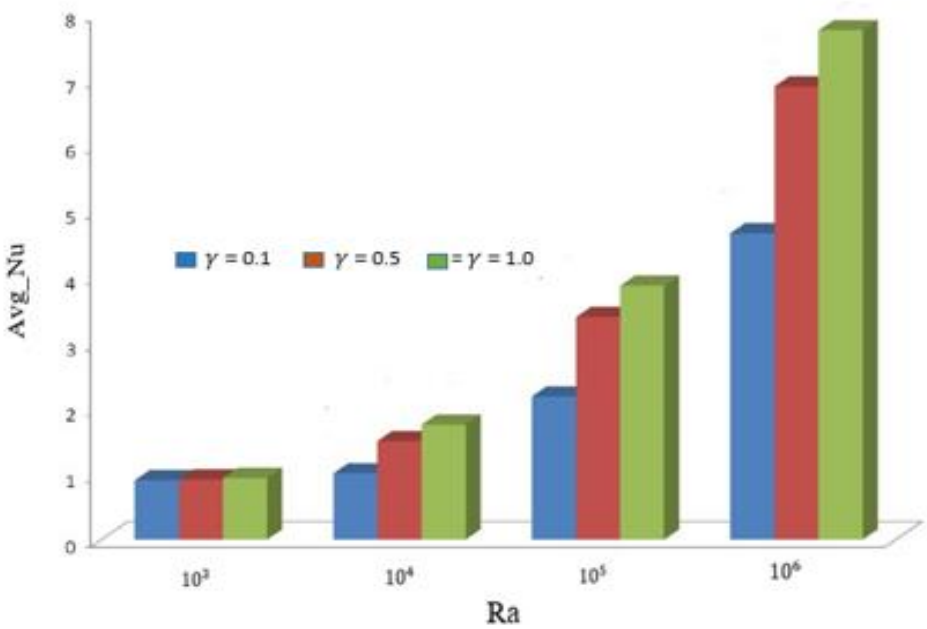

Figure 3b

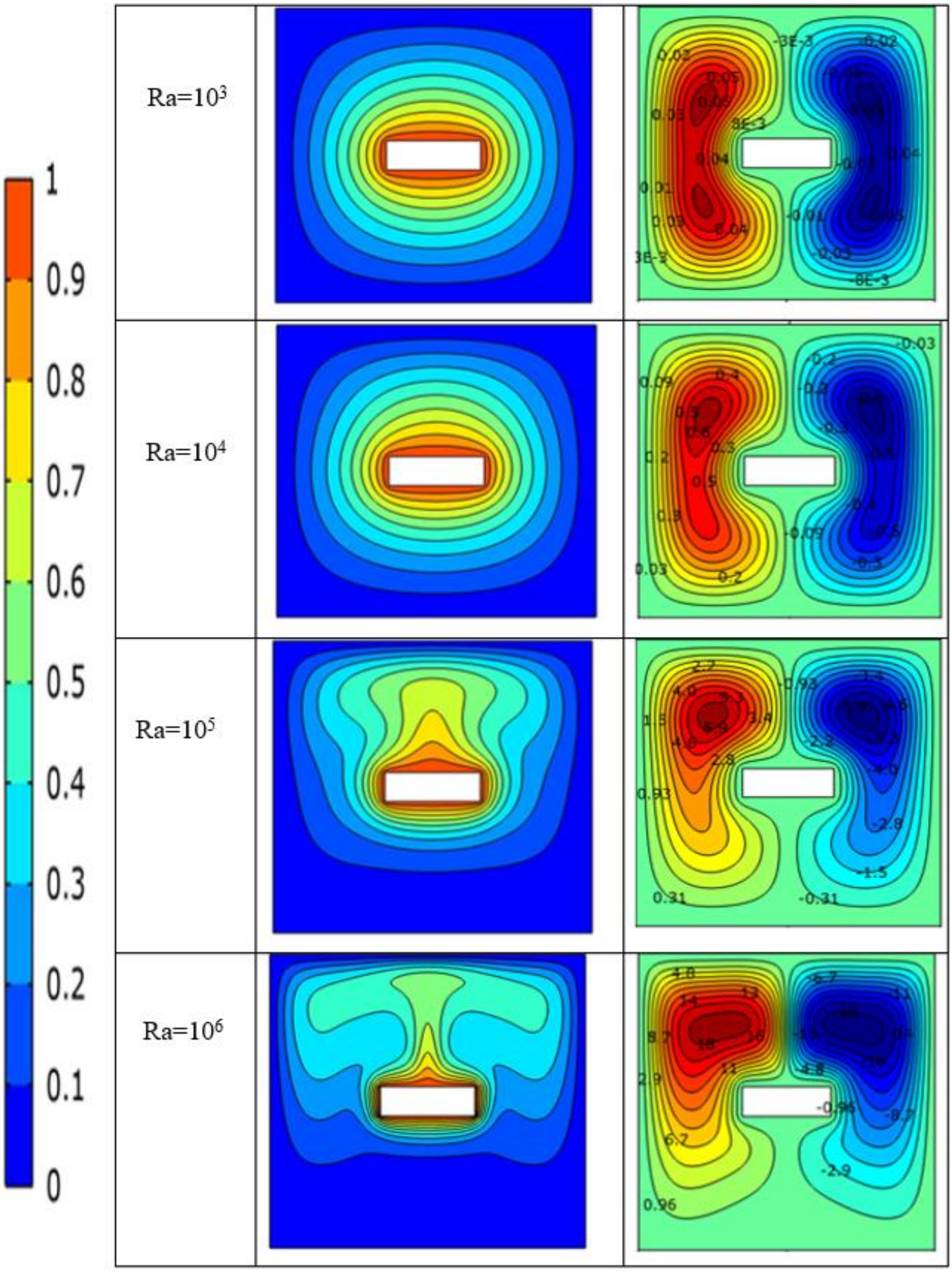

Figure 4

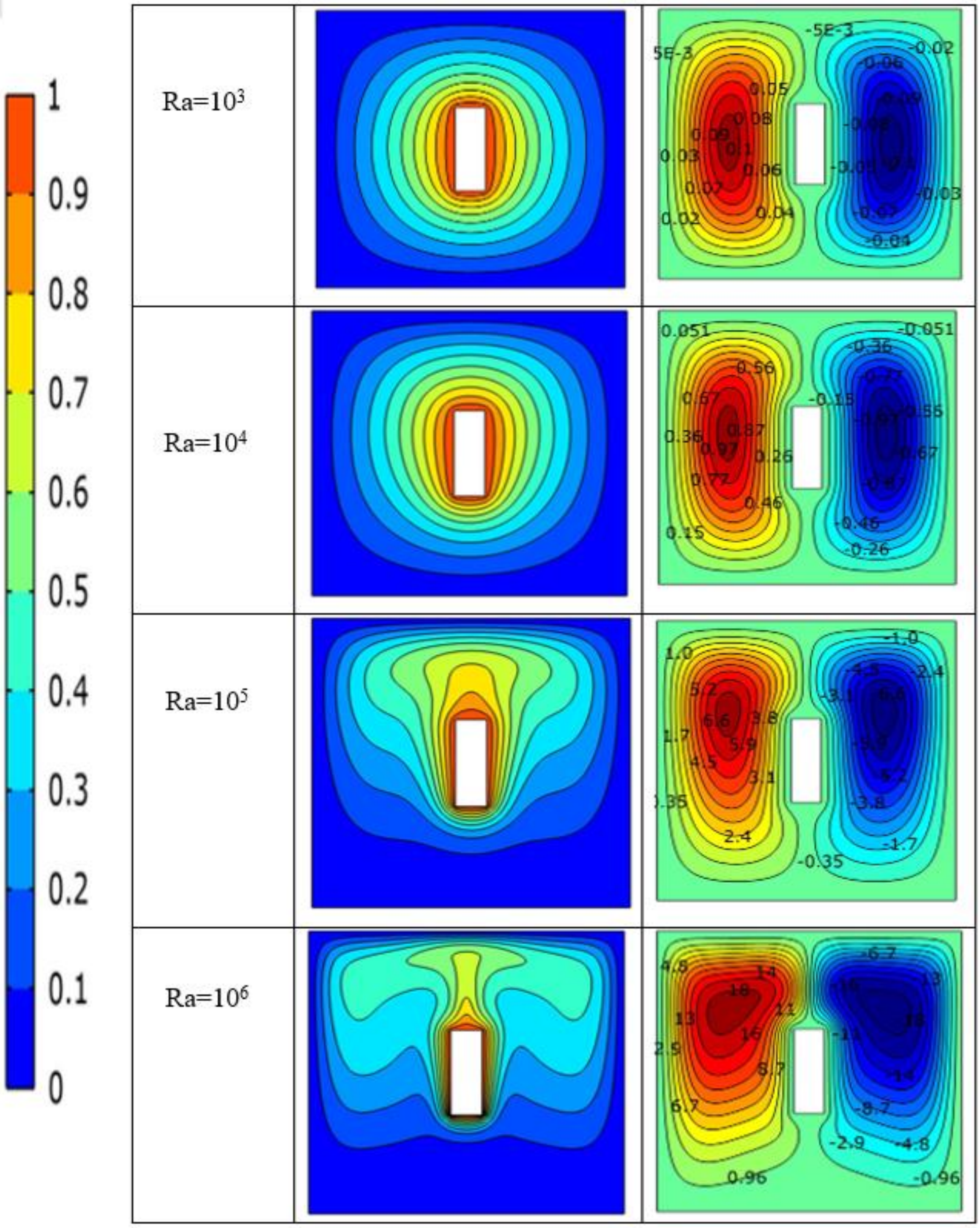

Figure 5

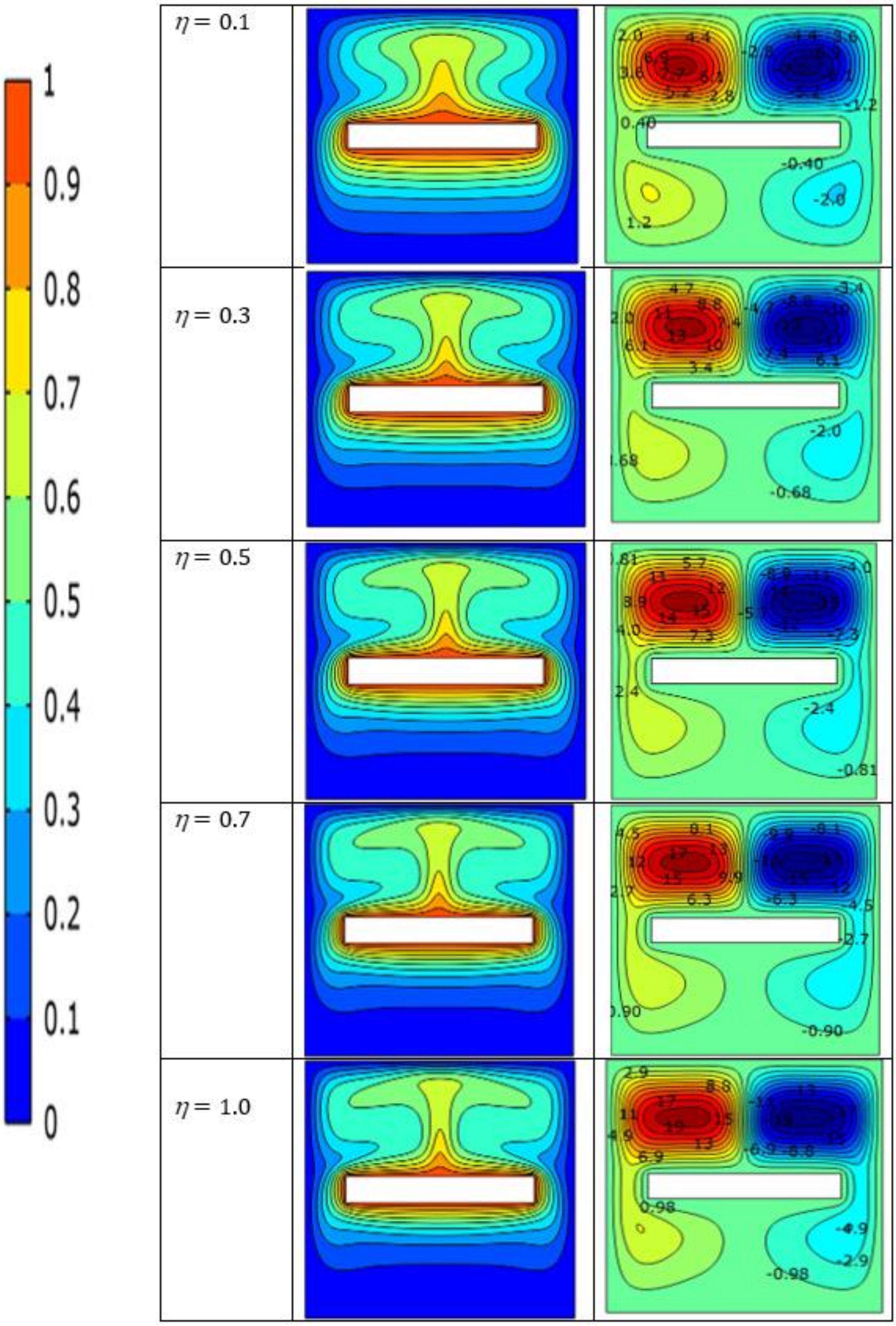

Figure 6

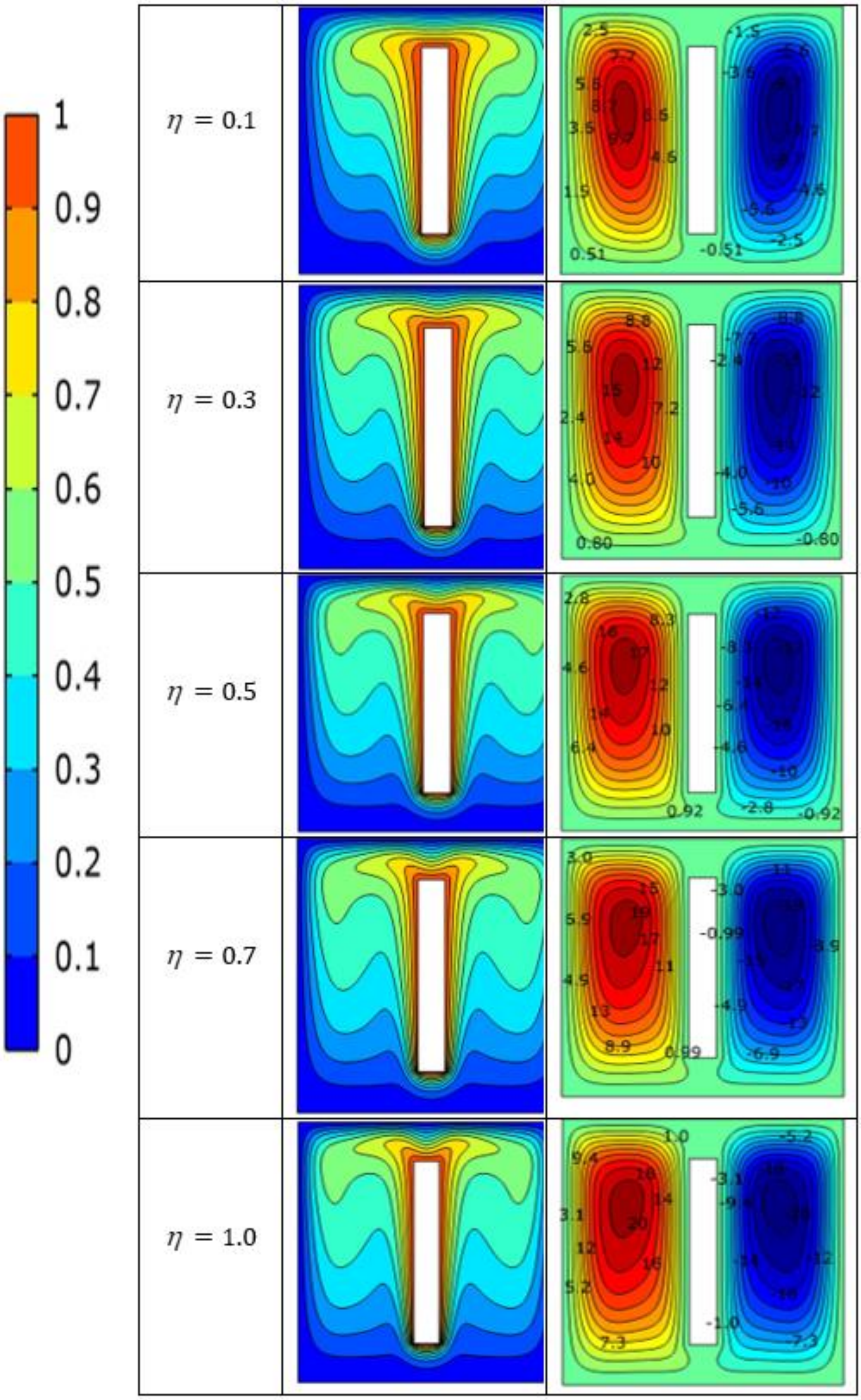

Figure 7

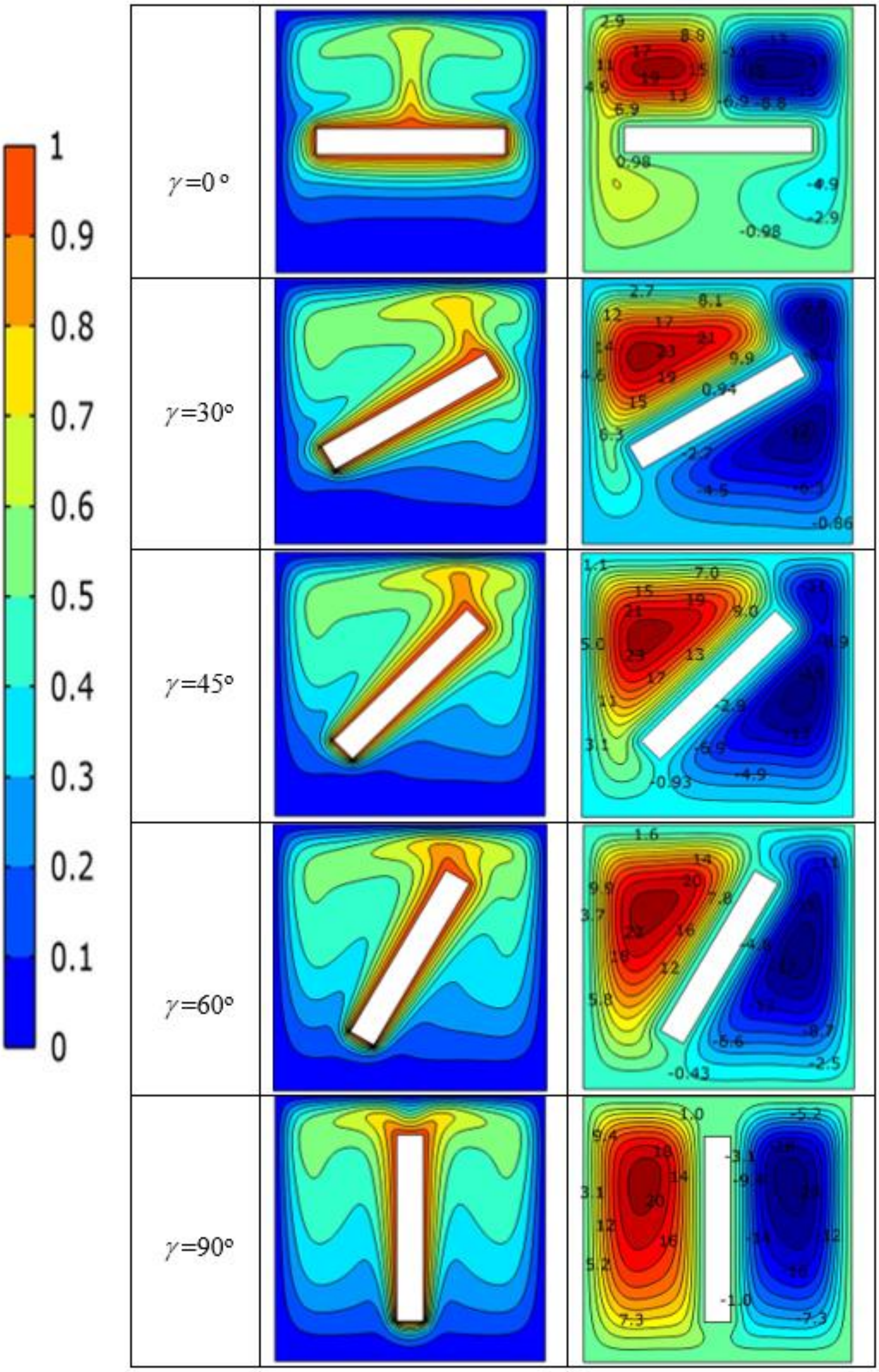

Figure 8

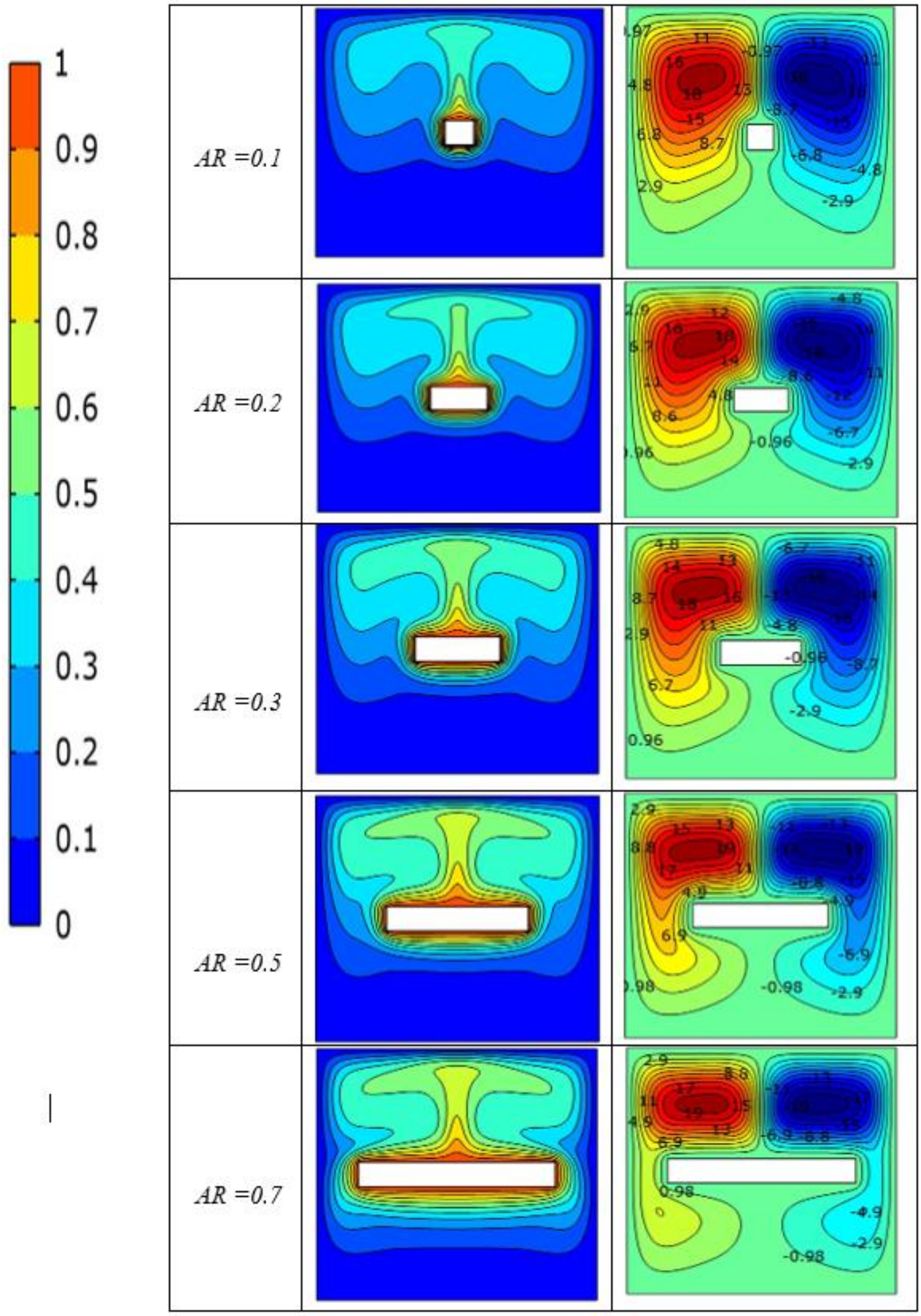

Figure 9

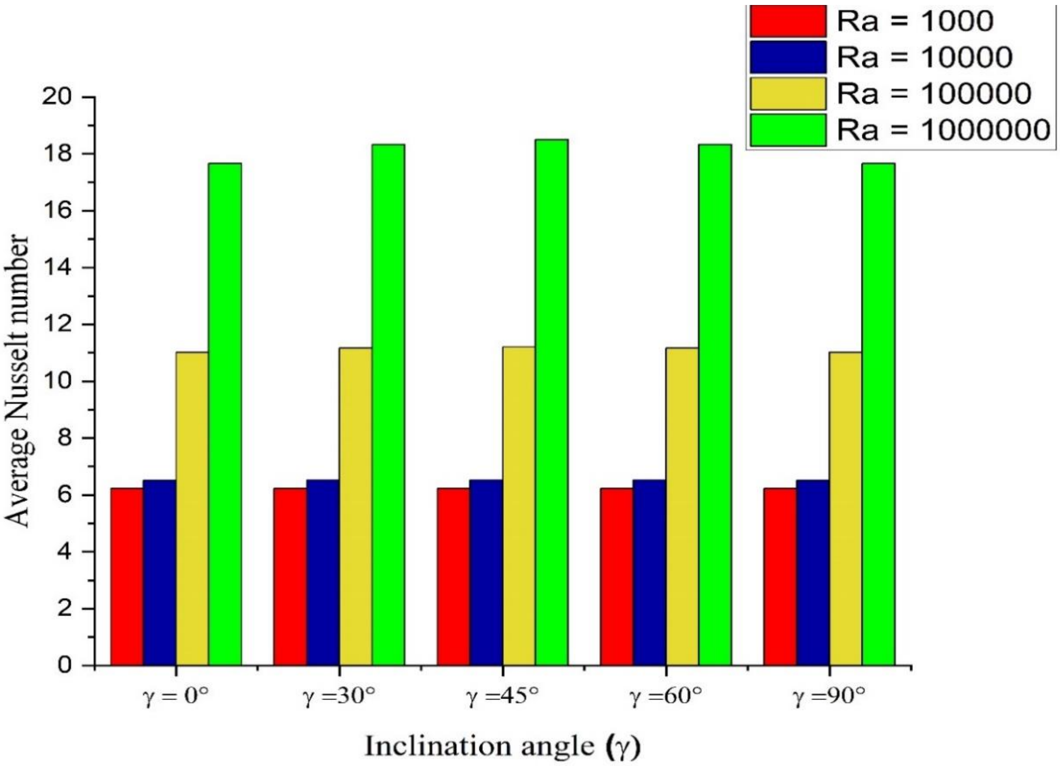

Figure 10

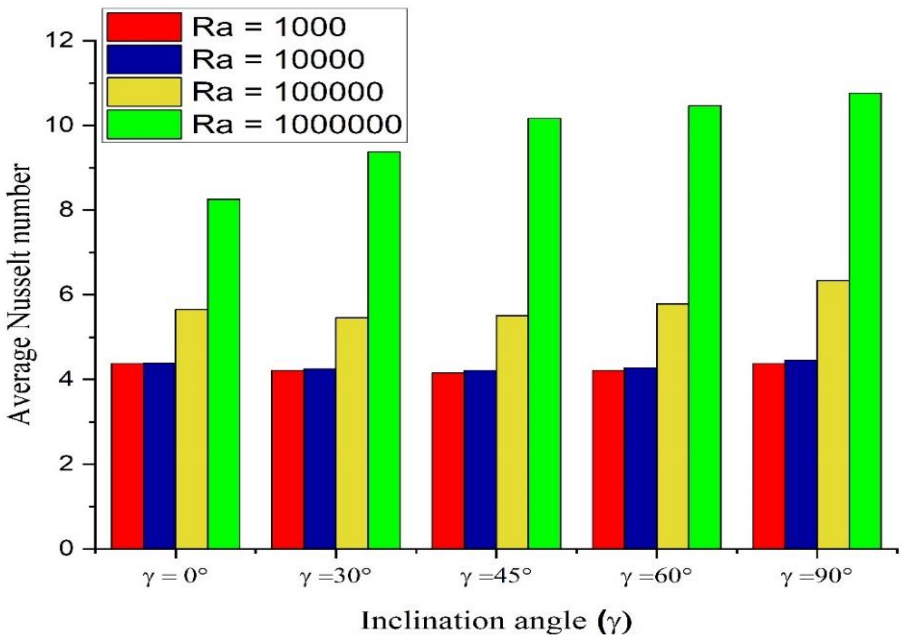

Figure 11

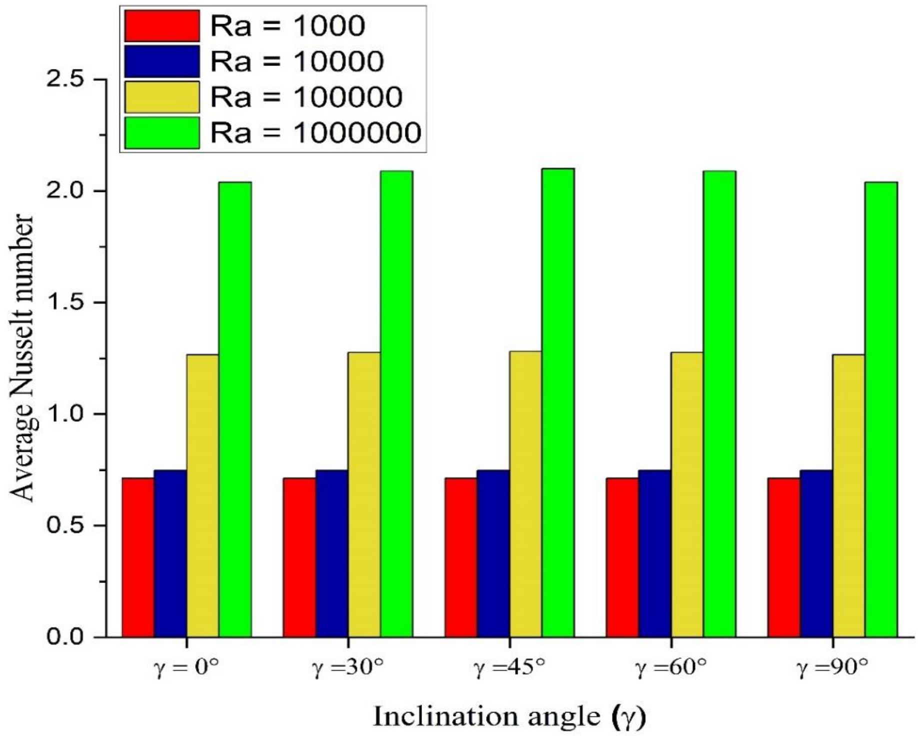

Figure 12

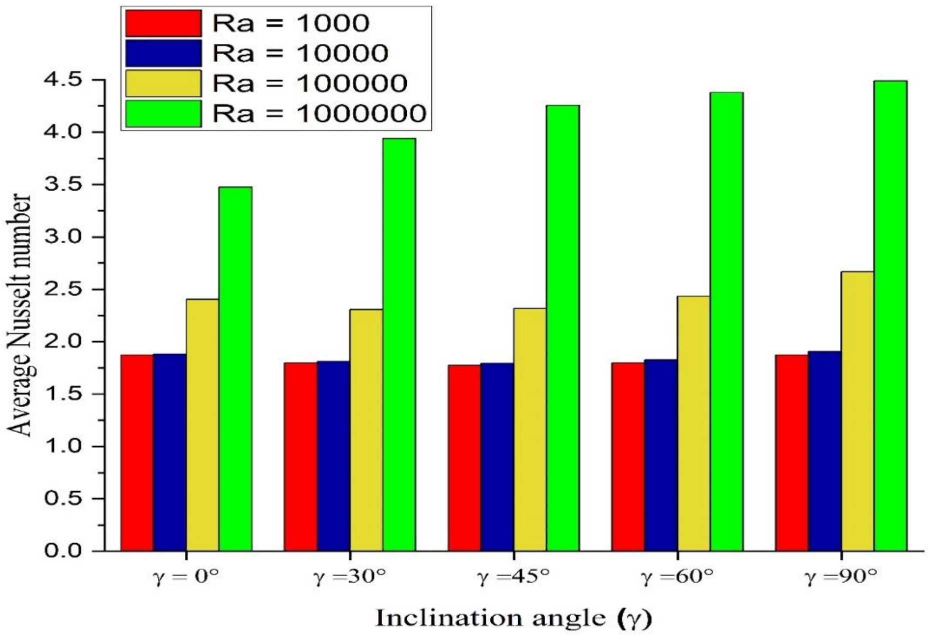

Figure 13

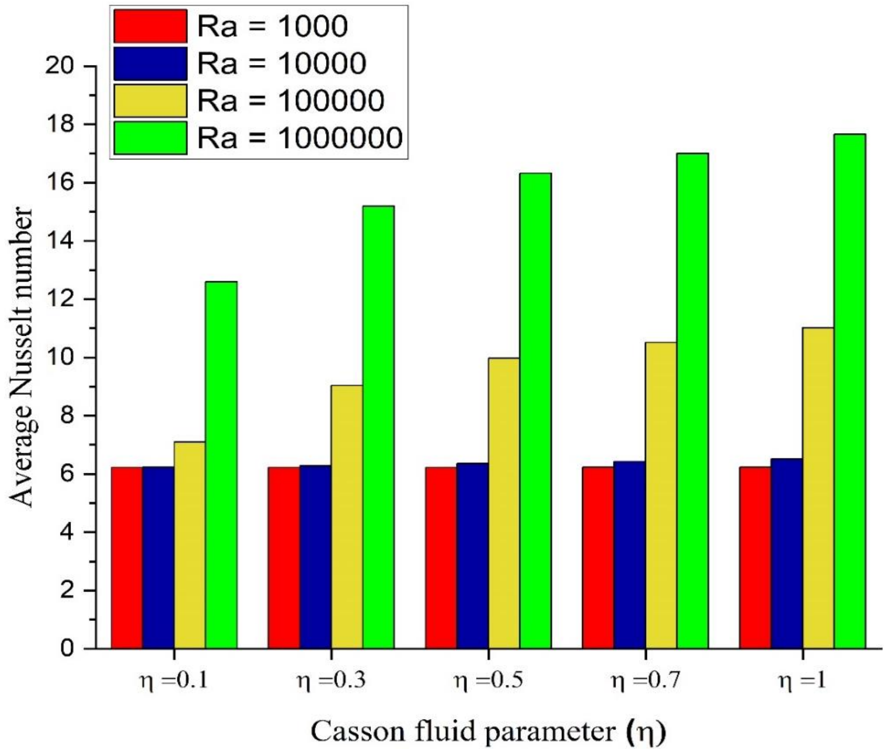

Figure 14

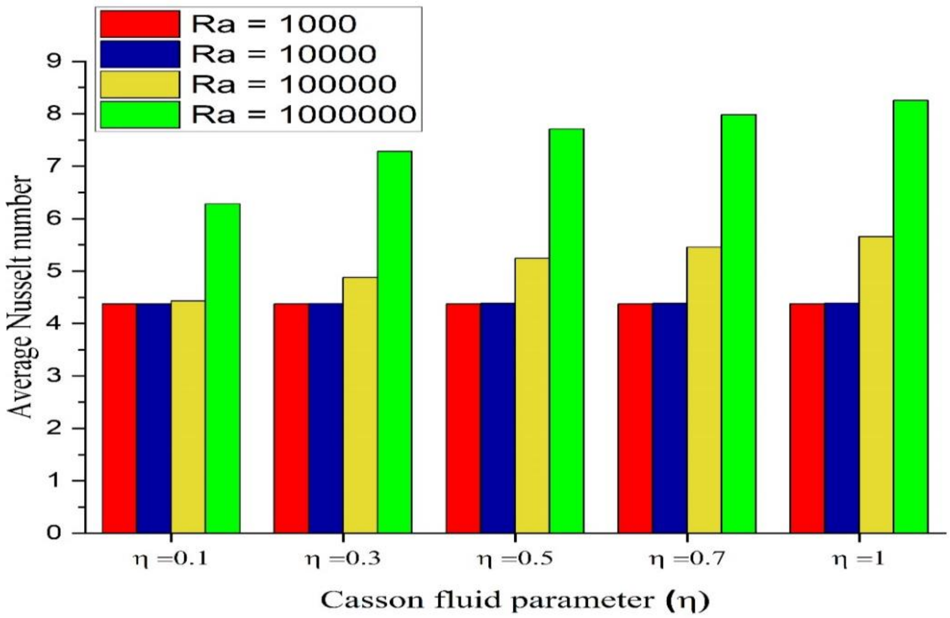

Figure 15

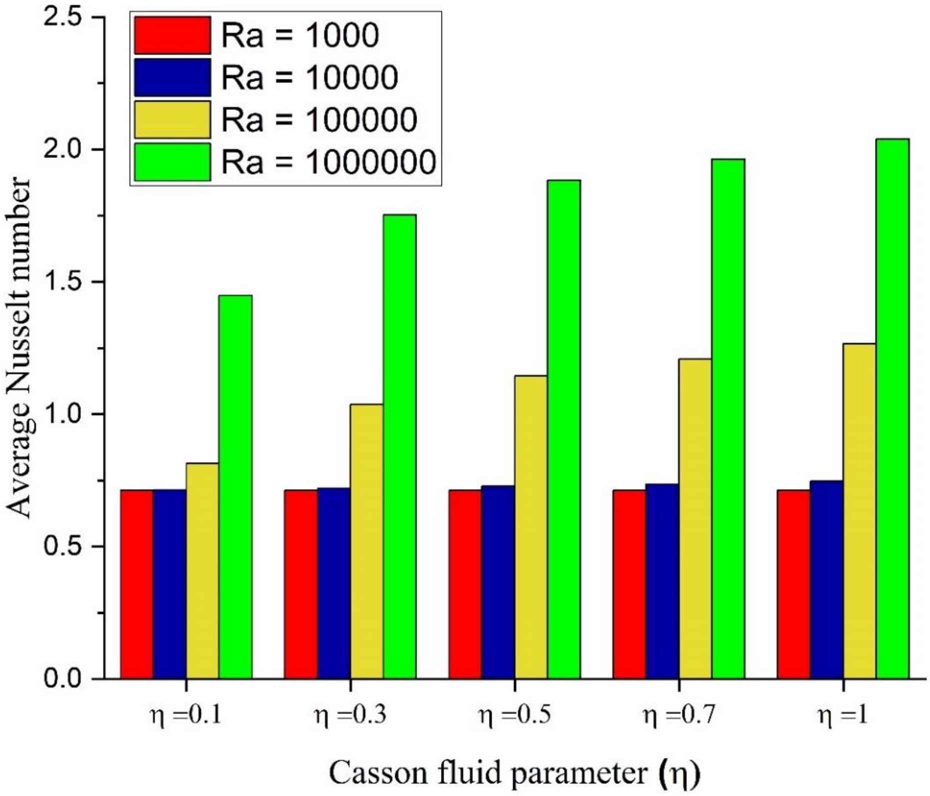

Figure 16

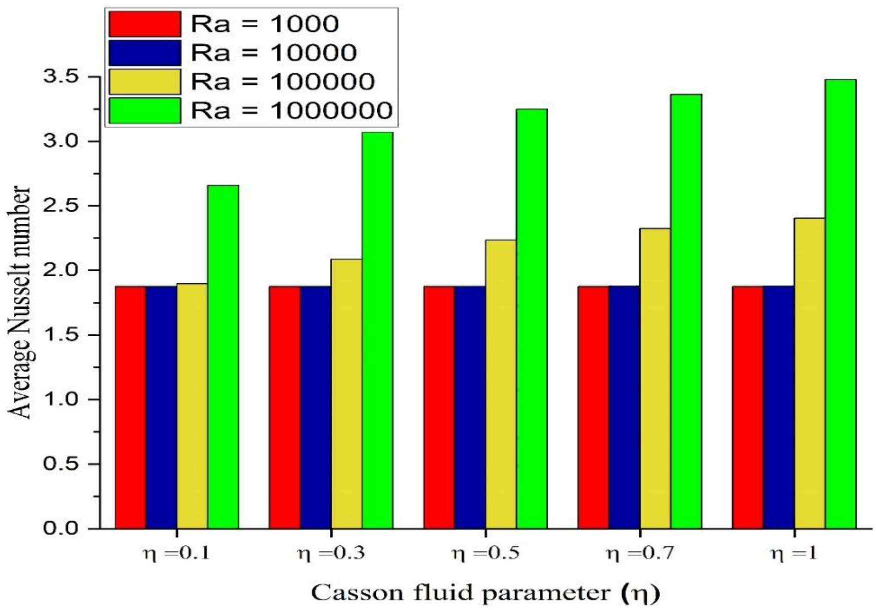

Figure 17

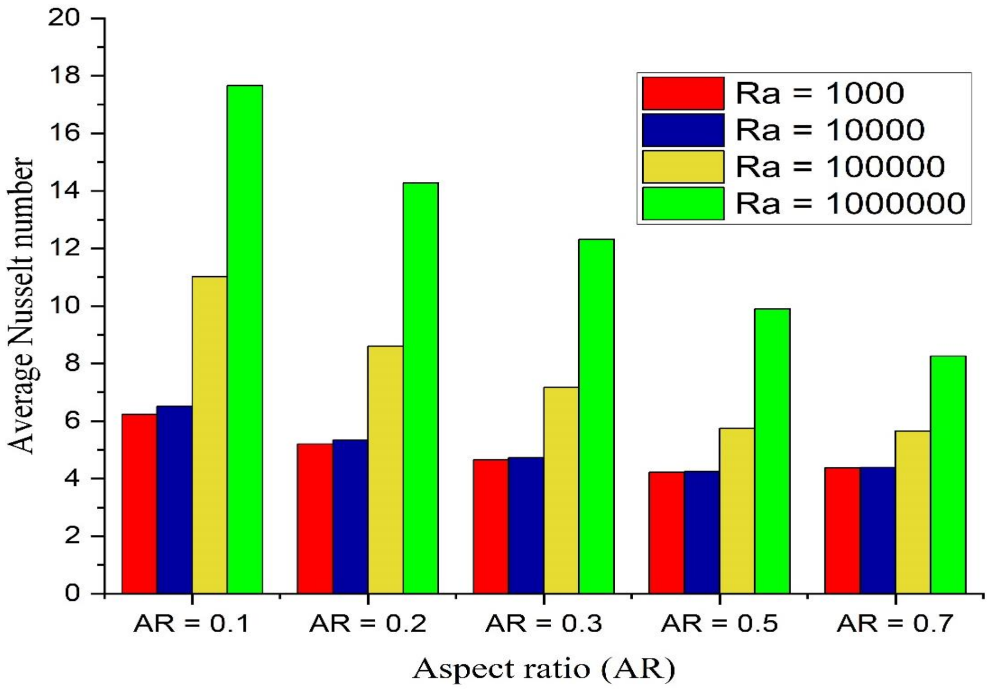

Figure 18

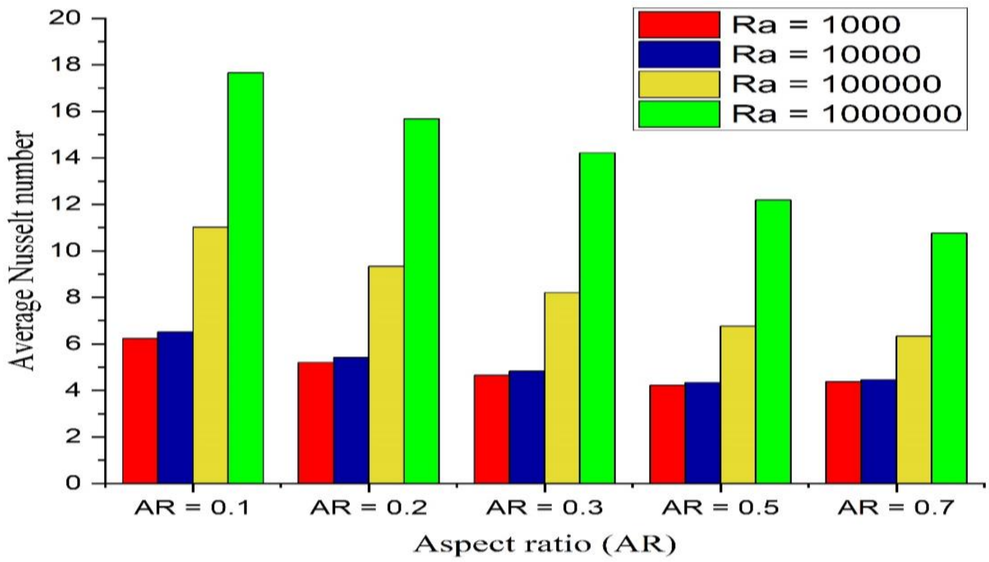

Figure 19

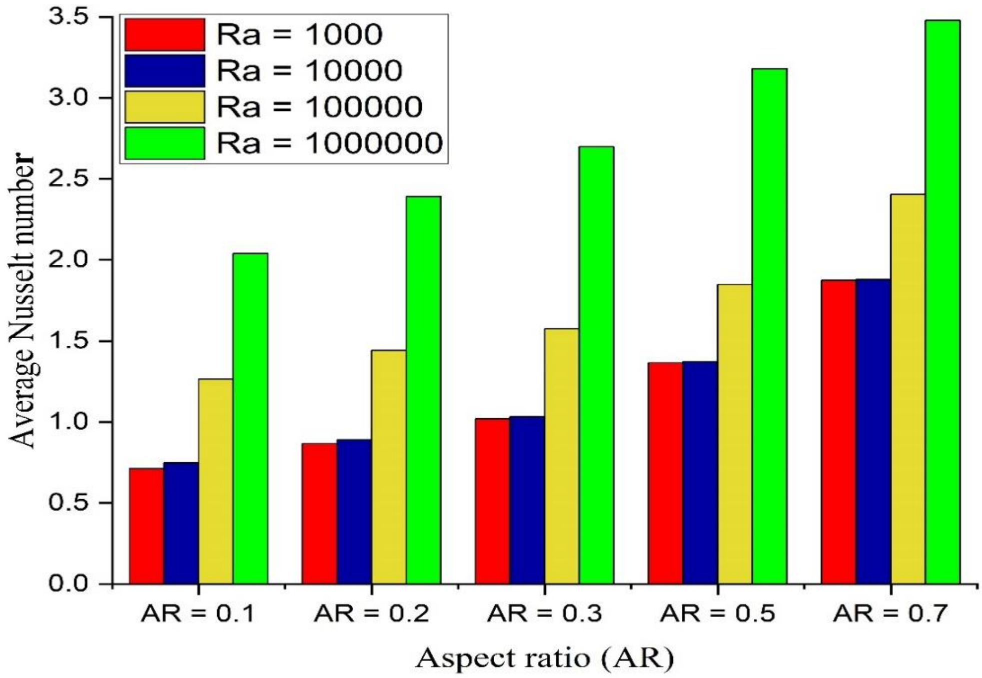

Figure 20

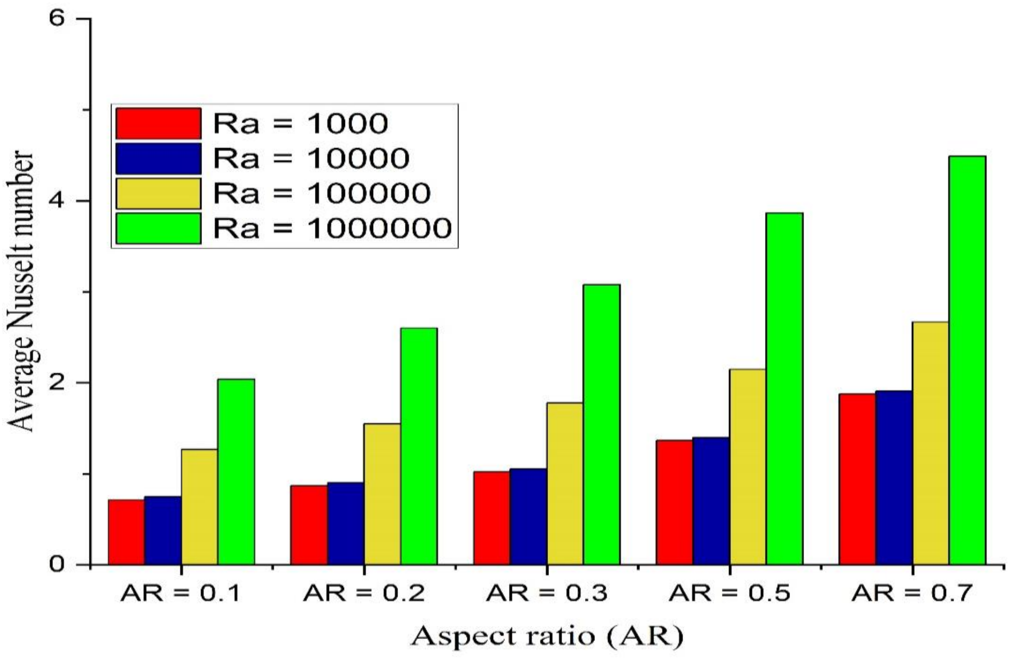

Figure 21

Biographies

Olalekan Adebayo Olayemi is currently a PhD Researcher at the School of Aerospace, Transportation and Manufacturing, Cranfield University, United Kingdom, and a lecturer in the Department of Aeronautical and Astronautical Engineering, Kwara State University, Malete, Kwara State, Nigeria. His research interests involve thermofluids, computational fluid dynamics, and Aerodynamics. He has published articles in peer-reviewed journals in his areas of interest. He is a member of the Nigerian Society of Engineers (MNSE) and a registered Professional Engineer at the Council for the Regulation of Engineering in Nigeria (COREN).

A.M. Obalalu is an applied mathematician specializing in various areas, including fluid dynamics, concentrated solar power (CSP), solar thermal systems, nanofluid heat transfer, solar nanofluid applications, and photovoltaic cooling. He has published numerous articles in reputable scientific journals. A.M. Obalalu has served as a member of the editorial team for various scientific journals, including the prestigious Green Electricity Journal. His contributions to the field of applied mathematics have been significant, and his expertise in various areas has made him an asset to the peer-review process and editorial team of scientific journals. A.M. Obalalu is lecturer in Department of Mathematical Sciences, Augustine University Ilara-Epe, Lagos, Nigeria.

T.F. Ajide holds a Bachelor of Engineering Degree in Aeronautical and Astronautical Engineering from Kwara State University, Nigeria. His research interests are in aerodynamics computational fluid dynamics, modeling and simulation, and heat transfer. He has published some articles in peer-reviewed journals. Currently, he is researching on vertical axis wind turbines for deployment in Ilorin, Kwara State, Nigeria. He is currently in the process of registering as a graduate student with the Nigerian Society of Engineers.

Dr. M.A. Ismael is a professor at the University of Basrah, College of Engineering where he got his B.Sc., M.Sc., and PhD in 1996, 1998, and 2007, respectively. He started his research field with electromagnetic flow measurement, then his passion turned into CFD, FSI, convective heat transfer of porous media and nanofluids. He has published about 60 papers in this field and won five prizes of a distinct researcher, two of the prizes is from Al-Eyen University award and three from the University of Basrah. Currently he works at the Department of Mechanical Engineering, University of Basrah. At the same time, Muneer Ismael is a visiting research fellow at the University of Warith Al-Anbiyaa, Karbala, Iraq. His current project is "Phase change modeling".